1978

Studies of negative ion-atom scattering at low collision energies

Barry T. Smith
College of William & Mary - Arts & Sciences

STUDIES OF NEGATIVE ION-ATOM SCATTERING AT LOW COLLISION ENERGIES

A Dissertation

Presented to

The Faculty of the Department of Physics

The College of William and Mary in Virginia

In Partial Fulfillment

Of the Requirements for the Degree of

Doctor of Philosophy

---

by

Barry T. Smith

September 1978

APPROVAL SHEET

This dissertation is submitted in partial fulfillment of

the requirements for the degree of

Doctor of Philosophy

Barry T. Smith
Author

Approved, September 1978

Roy L. Champion
Roy L. Champion

Lynn D. Doverspike
Lynn D. Doverspike

John B. Delos
John B. Delos

John R. Kane
John R. Kane

Eric Herbst
Eric Herbst
Department of Chemistry

This work is dedicated to my wife Marian whose understanding and strength of will carried me through the completion of my graduate school studies.

TABLE OF CONTENTS

LIST OF TABLES

LIST OF FIGURES

ACKNOWLEDGMENTS

The author would like to give his heartfelt thanks to his advisors Roy Champion and Lynn Doverspike who have patiently guided the author through his graduate studies. The writer is also indebted to John Delos for many helpful discussions, seminars and courses. Appreciation is also due the other members of the dissertation committee, John Kane and Eric Herbst, for their careful reading of the manuscript.

The writer also would like to thank Bill Vulcan and Stan Hummel for providing much needed support with the electrical and mechanical aspects of the experiments.

The writer also would like to thank Ruth Bryant for the typing of this manuscript.

ABSTRACT

The threshold behavior of the absolute total electron detachment cross section for collisions of Cl^- with He, Ne, Ar, Kr, H_2, D_2, O_2, N_2, CO and CO_2 has been determined in an ion beam-gas target apparatus. The measurements were completed over a relative energy range from below the electron affinity of Cl^- to approximately 150 eV. It was found that the threshold for detachment is about twice the electron affinity of chlorine. Relative elastic and inelastic differential cross sections were measured for collisions of Cl^- with O_2, N_2, CO and CO_2. The above experiments are discussed within the framework of a local complex potential model. This model is based on the assumption that the process for electron detachment is a result of the crossing of the Cl^- bound state with the continuum of neutral atom free electron states. Semiclassical calculations, using this model, are presented for the total detachment cross sections of Cl^- colliding with Ne, Ar and Kr.

Relative elastic and inelastic differential cross sections have been determined for collisions of Cl^- with Na and K as well as for collisions of H^- with Na. The measurements were completed over a relative energy range from 5 to 100 eV in an ion beam-gas target apparatus. For the systems Cl^- + Na(K) it was found that the cross section for ion pair production or electron detachment is very small when compared with the elastic scattering cross section. A semiquantal calculation is presented for the elastic differential cross section. The elastic differential cross section for H^- colliding with Na exhibited behavior characteristic of collisional detachment. All of these reactants have large dipole moments making possible bound negative molecular states; the data showed rainbow phenomena characteristic of scattering from bound states.

VITA

Barry T. Smith

Born on November 19, 1950; the author's hometown is Paulsboro, New Jersey. Graduated from Paulsboro High School in June 1968, B.S. in Physics from Duquesne University, 1972. The M.S. degree with a concentration in physics was awarded by the College of William and Mary in August of 1974.

STUDIES OF NEGATIVE ION-ATOM SCATTERING AT LOW COLLISION ENERGIES

I. INTRODUCTION

An experimental study has been made of collisions of negative ions with atoms and molecules at low relative collision energies. Absolute total cross sections have been measured for the process of collisionally induced electron detachment from the negative ion. Relative elastic and inelastic differential cross sections were also determined. These experiments were performed with an ion beam-gas target apparatus over a relative energy ranging from 2-150 eV.

The absolute total detachment cross sections were determined for collisions of Cl^- with He, Ne, Ar, Kr, H_2, D_2, O_2, N_2, CO and CO_2. Particular emphasis was placed on the region of the energetic threshold for electron detachment. Detailed experimental knowledge of the threshold region provides an essential test for collisional detachment models as well as for intermolecular potential calculations for negative molecular ions.

The differential cross sections measured were for collisions of Cl^- with O_2, N_2, CO, CO_2, K and Na as well as H^- with Na.

The collisional dynamics of negative ions and atoms are not only interesting from a purely academic viewpoint, but their interactions must be understood to comprehend the role of negative ions in many naturally occurring processes.

In the earth's ionosphere, processes leading to the formation and destruction of negative ions play mediating roles in the determination

of concentrations of electrons and various molecular species.[1] Negative ions are primarily formed by three processes:

1) three body attachment

$$X + M + e^- \rightarrow X^- + M$$

2) radiative attachment

$$X + e^- \rightarrow X^- + h\nu$$

3) dissociative attachment

$$XY + e^- \rightarrow X^- + Y$$

These reaction channels and their inverses leading to electron detachment, govern concentrations of electrons, positive and negative ions, and neutrals in the upper atmosphere. Knowledge of the cross sections and rate constants for these reactions leads to a better understanding of phenomena in the ionosphere. In the solar photosphere, the absorption spectra of H^- contributes to the observed spectral distribution.[2]

A full understanding of the plasma conductivity in Magneto-Hydrodynamic devices must include a consideration of possible negative ions in the plasma.[3] The formation and destruction of negative ions in the plasma affect the electron concentrations which are the most mobile charge carriers in the plasma.

One of the most promising approaches for heating the plasma of tokamak fusion devices is by injection of high flux, high energy neutral beams of deuterium atoms. The earliest method used was to create a positive deuterium ion beam which underwent charge transfer in an alkali vapor collision cell, $D^+ + Cs \rightarrow D^o + Cs^+$. This technique was limited by low efficiences at the high energies needed for injection

($E \sim 250$ KeV). Most recent efforts have focused on the production and neutralization of negative hydrogen ions and beams,[4] i.e., $D^- + X \longrightarrow D^o + X + e^-$.

In this study we have focused on the process of collisionally induced electron detachment from negative ions. An understanding of the dynamics of this inelastic reaction channel is an important step toward predicting the contribution of negative ions in the aforementioned processes.

The collision studies presented here also include alkali target systems. The alkali-halides and hydrides are interesting systems since the molecules have such large dipole moments. This fact has led to many ab initio and model calculations for the intermolecular potentials which predict stable negative bound states. The H^- - Na system is particularly interesting since part of the fusion effort has lately focused on creating negative hydrogen ions from alkali-coated surfaces.[5] The alkali is deposited as a mono-layer on substrates of Mo; when bombarded with H^+ or H^o some percentage of the backscattered product is in the form of H^-. This process is still under investigation and the study of elastic scattering of H^- + Na is of immediate use.

Chapter II will contain a description of the experimental apparatus. In Chapter III both ab initio potential calculations and collision model calculations will be reviewed. The absolute detachment cross sections determined for collisions of Cl^- with He, Ne, Ar and Kr are contained in Chapter IV. The results for the diatomic targets are contained in Chapter V. The experimental results for the alkali-halides

and the alkali-hydride reactants are in Chapter VI. A summary of results and conclusions can be found in Chapter VII.

II. EXPERIMENTAL APPARATUS AND METHODS

In the negative ion-atom (molecule) experiments completed, two different apparatuses were used. Absolute total detachment cross sections were measured on one machine, and the relative differential cross sections on another. The experiments employed gas phase targets and ion beams that had well resolved energy and spatial distributions. We will discuss the details of each apparatus separately and follow with a discussion of the methods used in data reduction.

A. Differential Cross Section Apparatus

A schematic diagram of the relative differential cross section apparatus is shown in Fig. 1. The ions are extracted from the ion source, accelerated, and focused into a magnetic momentum analyzer. Next, they enter the main vacuum chamber where a series of decelerating lenses focus the ions into the collision region. Beyond the collision region, there are the following: a 127° energy selector, radio frequency mass spectrometer, a charged particle multiplier and a neutral particle detector. The detection system beyond the collision region is capable of detecting particles that are scattered between -2° to 40° relative to the incoming ion beam. This detector configuration makes it possible to examine the elastic scattering channel and the inelastic channels for both fast neutrals and negative ions.

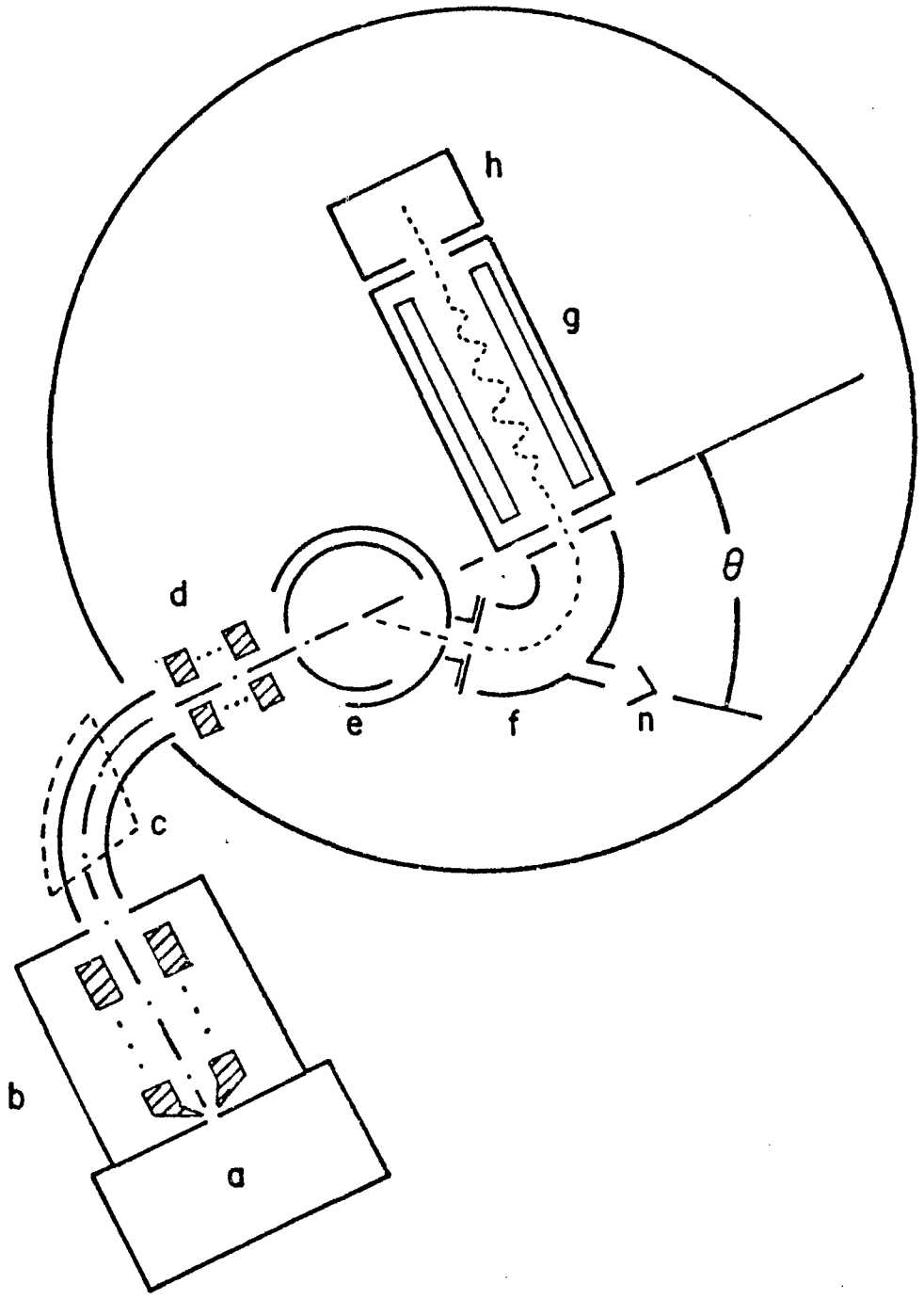

Figure 1. (a) ion source, (b) accelerating and focusing electrostatic lens system, (c) magnetic mass spectrometer, (d) retardation lens system, (e) collision chamber, (f) energy analyzer, (g) radio frequency mass spectrometer, (h) particle multiplier, (n) neutral detector. No attempt has been made to indicate the scale of the various elements.

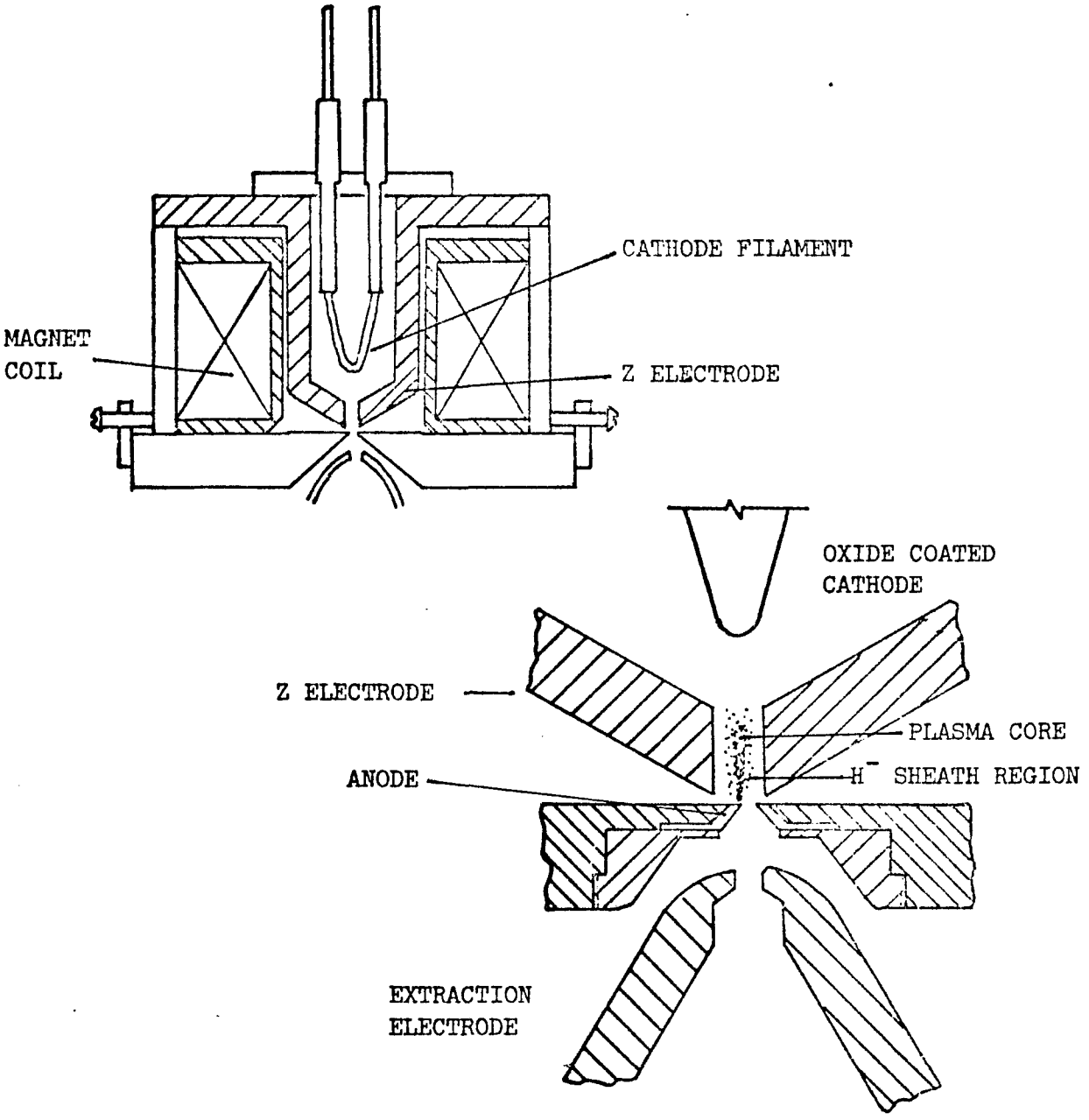

Figure 2. A cross sectional view of the duoplasmatron with a blow-up of the critical region showing the plasma core and negative ion sheath region. No scale is indicated.

Two types of beam sources were used in the relative differential cross section measurements. The H^- beam was produced with a duoplasmatron and the Cl^- beam with a surface attachment source.

Duoplasmatron

The duoplasmatron shown in Fig. 2 is similar in design to one described by Aberth and Peterson.[6] The filament is constructed of a rolled piece of nickel mesh, coated with a triple carbinate, (Ca_2CO_3, Ba_2CO_3, Sr_2CO_3 to lower the work function) and is mounted on a set of copper electrodes. The filament sits inside an intermediate (or Z) electrode. The Z-electrode is normally kept electrically shorted to the filament but to strike an arc, it is momentarily shorted to the anode potential. Coaxial with the filament and Z-electrode is a coil, whose magnetic field provides for focusing of the arc. The anode is a copper disk with an aperture of approximately 0.050 inches diameter mounted just beyond the Z-electrode. To strike an arc and create a beam of ions, the filament is heated by supplying approximately 18A at 1.5 VAC. The source gas is then admitted by a precision leak valve into the region of the filament. When the Z-electrode is shorted externally to the anode potential, an arc is temporarily struck between the Z-electrode and the filament; the arc is subsequently maintained between the Z-electrode and anode. To extract a large current of H^- from the sheath of this plasma, it has been found that the axis of the Z-electrode should be displaced laterally from the axis of the cathode by approximately 0.050 inches.[7] This offset cuts down the extraction of large electron currents from the source. When operating, the arc current is in the range from 0.15-1.5A.

For an H^- beam a source gas mixture of about 50% Ar and 50% H_2 is used. This combination seems to be useful for long term stability of the arc. Typical beam currents measured at the particle detector are a few nanoamps with an energy spread of 0.7 eV FWHM after passing through the momentum analyzer.

Surface Attachment Source

The phenomena associated with the creation of negative ions by surface attachment (or "surface ionization") have been described in the literature.[8] Fig. 3 is a schematic of the source used for the Cl^- beam.

At the top is an inlet for gaseous CCl_4 and inside the chamber is a filament and an electrostatic lens for extracting the ions. This extraction lens has its entrance covered with a 95% transparent tungsten grid, so as to produce a strong electric field for ion extraction. The filament is a thoriated iridium ribbon of the type used in vacuum gauges (Veeco No. 1220-003).

The surface ionization technique works for systems where the electron affinity (E.A.) of the atom is greater than the work function of the cathode. The relevant pathway for the formation of Cl^- seems to be molecular decomposition of CCl_4 on the hot filament, followed by an effusing negative halogen ion. The filament operates with a current of 5A which provides a surface temperature of approximately 1200°C. Pressure on the inlet side of the ion source is in the range from 0.05 to 0.15 Torr.

An energy analysis of a Cl^- beam was performed using a retardation technique on the total cross section apparatus, and the results are shown in Fig. 4. The dots are the experimental points; to these an error function was fitted, the derivative of which is a gaussian function. Shown is an ion beam with a primary energy of 6.3 eV and a FWHM of 0.06 eV. This relatively narrow energy spread and the fact that the filament potential was -6.5 volts indicates that the Cl^- ions are formed in the immediate vincinity of the filament.

For both the dupolasmatron and the surface attachment source, the kinetic energy of the ion beam is controlled by the potential difference between the cathode and earth ground, since the ions are formed near the cathode and are accleerated to the collision chamber which is maintained at ground potential.

Ion beam currents produced in both sources range from several nanoamperes at high energy, to a few tenths of a nanoampere at low ion beam energies.

Electrostatic Lens and Momentum Analyzer

Immediately following the ion source there is a set of electrostatic lenses[9] which extracts the ion beam and accelerates the ions into the magnetic momentum analyzer.

The momentum analyzer is a 90° X-band waveguide with a 6 inch radius of curvature with entrance and exit slits of dimension 0.050 x 0.50 inches, giving an approximate resolution of 60. The magnetic field is provided by an electromagnet with shaped pole pieces of the same

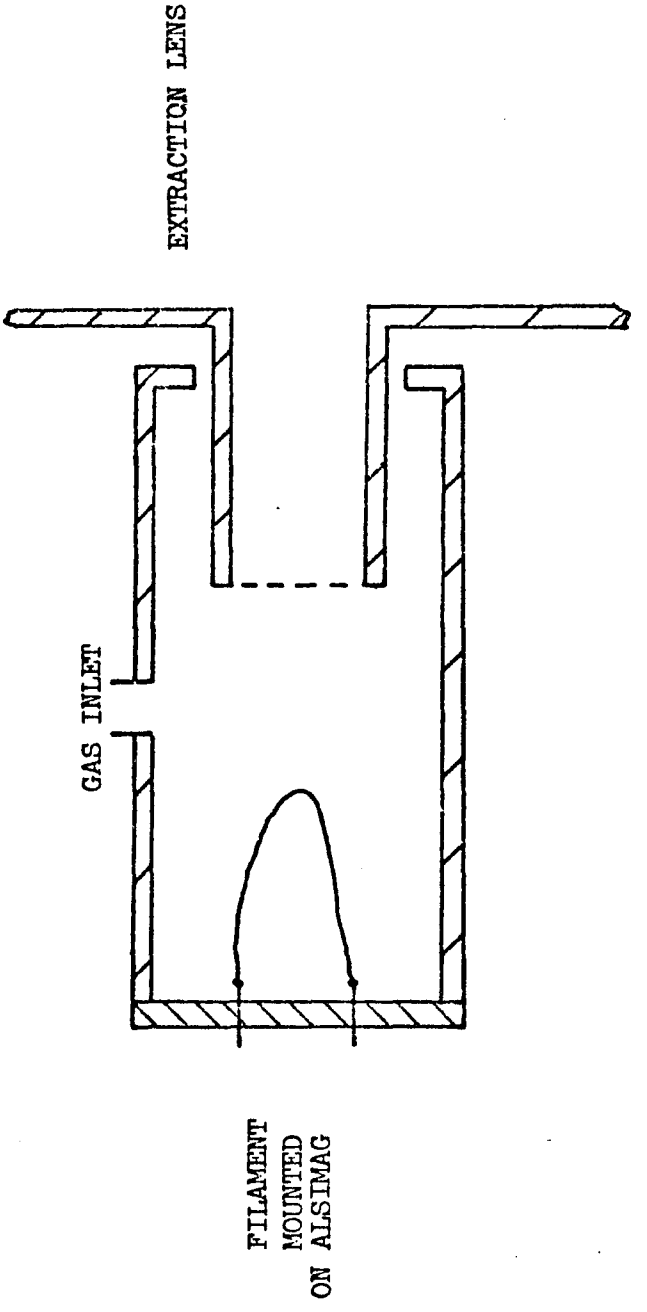

Figure 3. A schematic representation of the surface attachment source.

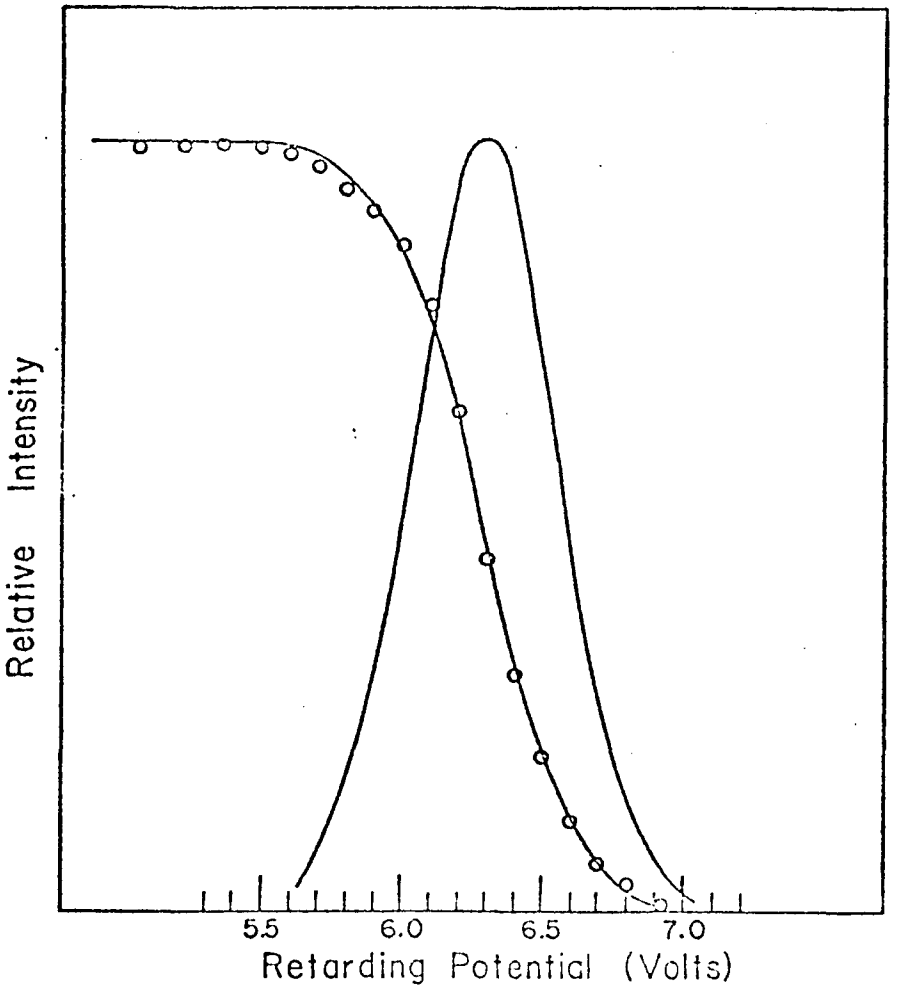

Figure 4. Retardation analysis used to determine energy distribution of negative ion beam. The open circles are experimental points and an error function which is fitted to these points is shown as a line. The derivative of the error function (a Gaussian function) gives the energy distribution of the primary ion beam.

approximate radius. The resolution is such that for the well defined energy of the surface attachment source, the spectrometer easily resolves the isotopes of chlorine (Cl^{35}, Cl^{37}).

The spectrometer injects the momentum analyzed beam into the main vacuum chamber, where there are another series of electrostatic lenses. These provide deceleration and focus the beam into the collision region. All of the electrostatic lenses are biased by the cathode power supply, so that once the ion beam is properly focused, if the energy is changed by raising or lowering the cathode potential, it is unnecessary to readjust the focusing conditions.

Collision Region

The collision region is defined by a stainless steel cylinder whose inside diameter is 0.85 inches. The entrance aperture is 0.125 x 0.035 inches, and the scattered product can exit by a 0.125 inch high slot cut from 0^{o} to 90^{o} relative to the primary beam. Over this cylinder is a coaxial rotating sleeve of brass construction which defines the laboratory scattering angle. It has an exit slit of 0.125 x 0.035 inches.

Two heaters, constructed of approximately ten inches of 35 guage nichrome wire would on ¼ inch diameter forms of Alsimag are mounted in the base of the collision chamber. A thermocouple of chromel-alumel is mounted between the heaters to monitor the temperature of the collision chamber.

These heaters are connected in series to a regulated DC power supply. Applying approximately 12 watts to the heaters brings the collision chamber to the proper temperature. By reducing the wattage slightly

when the chamber has reached the proper temperature, the temperature can be stabilized. During an experiment the temperature never drifted by more than 1K.

For all targets, the gas pressure in the collision region was kept in the range below 10^{-3} Torr. For the alkali targets this meant providing a temperature of 440K for potassium and 510K for sodium.[10] For the diatomic targets, a gas inlet was connected to the collision chamber and a precision leak valve was used to regulate gas flow.

Detection System

Following the collision region is a one inch long grounded drift tube, with the end farthest from the collision chamber covered with a 95% transparent tungsten grid. This grid eliminates electric fringe fields from the collision region.

The drift tube is mounted on, but electrically isolated from the face of an electrostatic energy selector, whose properties are well known.[11] The selector consists of 127° 17' coaxial cylindrical sections with radii of 3 cm. and 4 cm. The entrance and exit slits each have a dimension of 0.035 x 0.25 inches. External switching of the selector polarity makes it possible to pass both positive and negative ions. The entrance slit is electrically isolated and it can be used to accelerate or decelerate ions into the energy selector, making possible inelastic studies and facilitating elastic studies. During experiments, the energy selector is tuned to pass the primary ion beam at 0° with no scattering gas in the chamber. The selector is kept at the same energy setting

since its transmission coefficient for different energies is unknown, and the ions are accelerated or decelerated as needed for elastic scattering angular profiles or inelastic spectrum studies.

After leaving the energy selector the ions enter a radio frequency mass spectrometer[12] (RFMS). A particle detector (Bendix 306 electron multiplier) whose design and operating characteristics have been well documented[13] is mounted at the exit aperture of the RFMS. The output of this detector can be monitored as DC current on an electrometer or, when externally switched, in a pulse counting mode. In the pulse counting mode, the output is capacitively coupled to a charge sensitive preamplifier, followed by a linear amplifier which also shapes the pulse, and this signal is fed to a single channel pulse height analyzer-scaler. After accumulating counts on the order of 20 seconds the scaler output is fed into a teletype printer system. Common background levels are a few counts in ten seconds.

To detect fast neutrals, a Channeltron Electron Multiplier[14] (CEM) is used. The CEM is mounted on the outer wall of the 127^{o} energy selector. A hole is drilled through this outer section such that when the CEM is mounted, it is in the direct primary beam line when the detection system is rotated to sample 0^{o} relative to the incoming primary beam. The output of the multiplier (CEM) is fed into a preamplifier, then to a linear amplifier-pulse shaper, and into a scaler-analyzer. Background noise for this system is on the order of one or two counts in ten seconds. The absolute detection efficiency for neutral particles in the CEM is not known for the experiments reported here. Even though only relative differential cross

section measurements were performed in the efficiency of the CEM as a function of the neutral particle's energy may be important in some cases. Morgenstern et al.[15] determined that for a 20 eV ground state He atom, this detection efficiency was less than 10^{-3}; this value was determined relative to He^{+} efficiency at the same energy. They showed that from 100 eV to 20 eV the efficiency goes down by two orders of magnitude. Thus, at a particular energy, an angular profile of scattered fast neutrals may have an efficiency factor which decreases with increasing scattering angle.

The entire detection system is mounted on a table which pivots about the center axis of the collision chamber. The exit slit which defines the scattering angle is mechanically coupled to this table such that the exit slit of the collision region and the entrance slit of the velocity selector are in parallel planes, each having a normal plane which bisects the center of both apertures simultaneously.

The laboratory scattering angle is determined by a potentiometer system. A wiper connected to the rotating table slides along a precision resistor wire which carries a constant current. By measuring the voltage between the wiper and one end of the wire the scattering angle can be determined to within one-tenth of a degree. The scattering cross sections reported here are sampled in one-half degree steps. The nominal angular spread of the primary ion beam is approximately one degree FWHM.

Vacuum System

Because well resolved low energy ion beams are needed for the experiments reported here, very clean vacuum techniques are necessary. All lenses, analyzer and entrance and exit slits are coated with Aquadag after very careful cleaning of the components. Aquadag is graphite which is applied as a colloidal suspension in alcohol. When painted on, the graphite apparently minimizes space charge buildup on the lens element surfaces.

The apparatus vacuum system consists of two sections: a main chamber and an ion gun chamber which are connected by the momentum analyzer tube. The ion source and first lens stacks are contained in an aluminum box that is 14 x 5 x 6 inches. This section is pumped by two 2-inch, 30 liters/sec. mercury diffusion pumps which are liquid nitrogen (LN_2) trapped and backed by a mechanical fore pump.

The main vacuum chamber which contains the collision region and detection system is housed in an aluminum cylinder with a diameter of 28 inches and a height of 24 inches. This chamber is evacuated by a LN_2 trapped six inch, 260 liters/sec mercury diffusion pump that is backed by a mechanical fore pump. An ionization gauge monitors the pressure in this chamber which is $\simeq 10^{-6}$ Torr when experiments are being done.

B. Absolute Total Detachment Apparatus

The apparatus used in the absolute total electron detachment cross section measurements is shown in Fig. 5. The ions are extracted from a surface attachment source, focused through a Wien Filter and then into the collision region.

The beam source is of the surface attachment type and is identical to the one previously described. An extraction and three focusing electrostatic lenses focus the beam through the Wien Filter.[16] The device is an $\vec{E} \times \vec{B}$ field type spectrometer supplied by Colutron Corporation. The effective collision region is in cup B (cylindrical brass cup 3 inches in diameter and 1.75 inches long). Defining the far end of the collision region are three parallel grids (I, II, and III) separated by .15 inches which are made of 95% transparent tungsten mesh. Element C is used as a Faraday cup to monitor the intensity of the primary beam. Around cup B are wound 33 turns of No. 18 magnet wire which provides an axial magnetic field of about 6 gauss with an applied current of 1.5A. This provides one part of a trap for detached electrons, which are collected on element A.

The target gas is admitted through the top of cup B. The gas handling system has a two-inch oil diffusion pump which is LN_2 trapped to pump out an intermediate holding tank. Thus, by pumping out this ballast tank to 10^{-6} Torr before filling, the target gas purity is not downgraded from the specifications of the manufacturer (commonly 99.99%) The gas is metered by a precision leak valve into a U-tube which can be immersed in LN_2. This provides a further safeguard against contamination by condensible background gases. The gas flows from the U-tube directly into cup B.

The target gas pressure is monitored by an MKS Baraton Capacitance Manometer (type 145 BHS-1, 1 MM head). The manometer calibration was checked by a mercury manometer technique[17] and found to be accurate to within 5%. This is in agreement with reports in the literature[18]

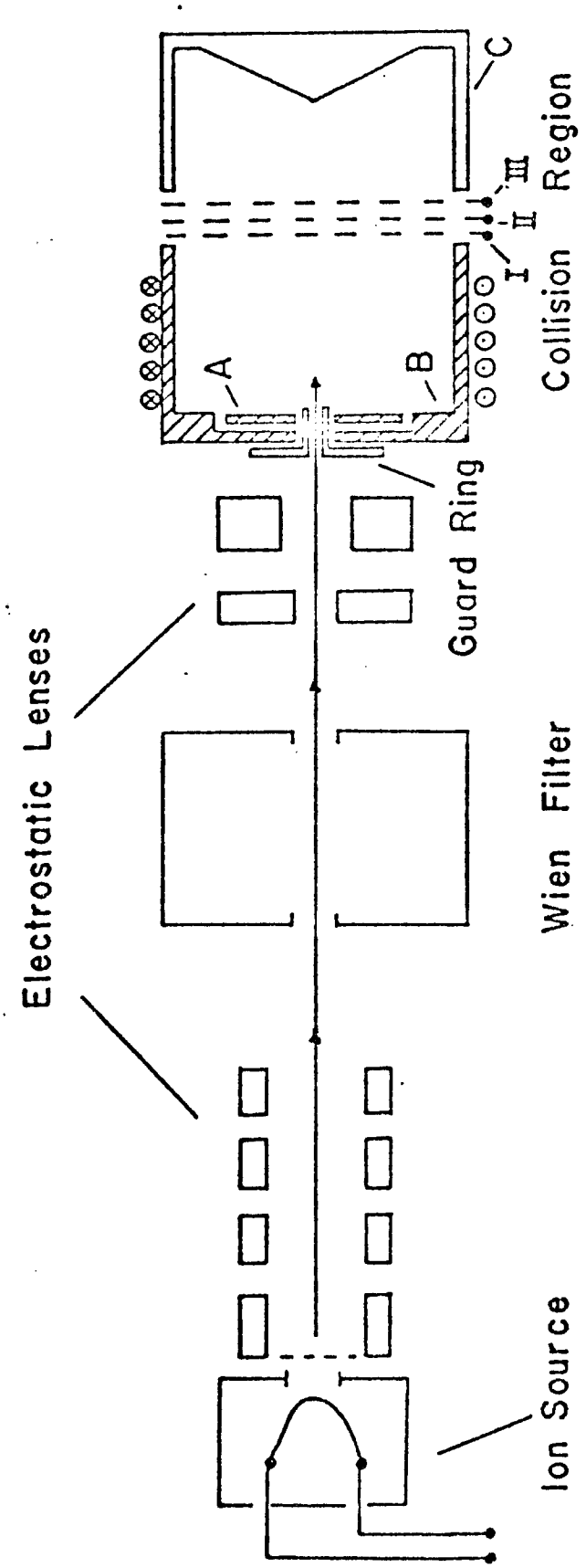

Figure 5. Schematic diagram of the total cross section apparatus.

and the manufacturer's claim of $\pm 5\%$ of the absolute pressure. Common target pressure at a constant leak rate was 4×10^{-4} Torr.

To provide for differential pumping the collision region is separated from the ion source by a baffle plate with a 0.1 inch entrance aperture. The ion source is pumped by a LN_2 trapped 6-inch oil diffusion pump (1500 liter/sec) and the collision region is pumped by a 4-inch LN_2 trapped oil diffusion pump (800 liter/sec).

Pressure is monitored by ionization gauges at the ion source and in the collision region. Also when pumping down the target gas handling system, an ionization gauge monitors the pressure. The inlet to the ion source has a thermocouple gauge to monitor the leak into the source.

As stated earlier, the target gas pressure is usually in the range of 10^{-4} Torr during experiments; background pressure before the scattering gas is admitted is typically 10^{-8} Torr in the collision region. Pressure on the ion source side of the dividing baffle is 10^{-6} Torr when the ion source is in operation.

C. Data Acquisition and Reduction

To facilitate analysis of the data it is convenient to convert the measurements taken in the laboratory into the center of mass (C.M.) coordinate system. Because the results reported here are from two entirely different measurements, it is convenient to discuss separately the procedures used in the analysis of the experiments along with estimates of the errors involved.

Differential Cross Sections

Since the measurements are relative differential cross sections, we must insure that the scattering signal can be suitably corrected for any systematic signal variation with scattering angle. Also the procedure for converting the experimental data to the center of mass reference frame must be clearly defined.

In order to clarify the discussion, consider the general scattering equation $M_1 + M_2 \rightarrow M_3 + M_4$ where the subscripts denote the projectile, target, detected fast product and undetected slow product, respectively. In such a collision the conservation of energy in the laboratory reference frame can be expressed as, $E_1 + E_2 + \Delta E = E_3 + E_4$, where E_1 is the relevant kinetic energy and ΔE is the change in internal energy of the particles: $\Delta E = U_1 + U_2 - U_3 - U_4$. For inelastic collisions where the internal energy undergoes some change, a positive value of ΔE is defined as exothermic and a negative change as endothermic.

The collision must also conserve linear momentum and the result of combining this with the conservation of energy yields:

$$\Delta E = \left(1 + \frac{M_3}{M_4}\right) E_3 - \left(1 - \frac{M_1}{M_4}\right) E_1 - \frac{2}{M_4} \left(M_1 M_2 E_1 E_3\right)^{\frac{1}{2}} \cos\theta$$

where θ is the laboratory scattering angle of M_3.

Likewise, the energy of the scattered particle can be expressed in the form

$$E_3 = \frac{M_1 M_3}{(M_1 + M_2)^2} \left\{\cos\theta \pm \left[\frac{1}{\gamma^2} - \sin^2\theta\right]^{\frac{1}{2}}\right\}^2 E_1$$

where:

$$\gamma = \left\{ \frac{M_1 M_3}{M_2 M_4} \quad \frac{E}{E + \Delta E} \right\}^{\frac{1}{2}}$$

and E is the energy in the center of mass frame of reference. A negative sign in the above equation corresponds to backscattering and a positive sign to forward scattering in the center of mass.

Earlier in discussing the velocity selector it was pointed out that since the transmission coefficient was not known, the elastically scattered particles were accelerated up to the primary beam energy. This requires an accelerating voltage of $E_1 - E_3$ and from the equation for E_3 the voltage can be calculated as a function of laboratory scattering angle.

The above discussion is strictly for binary-binary collisions, and is not strictly valid for all collision channels we consider. In the case of detachment $A^- + B \rightarrow A + B + e^-$, the outgoing channel involves three particles. However, the momentum carried by the electron is small and can be neglected, thus leading to approximately the same form for $E_3(\theta)$.

The equation relating the C.M. scattering angle (χ) to the laboratory scattering angle is:

$$\tan \theta = \frac{\sin \chi}{\gamma + \cos \chi}$$

Differential cross sections measured in the laboratory must be transformed into the center of mass cross sections. The relation between the two is that the number of particles scattered into the laboratory solid angle must equal the number scattered into the corresponding center

of mass solid angle. This transformation as a function of angle takes the form, $\sigma_{cm} = F \cdot \sigma_{lab}$, where

$$F = \frac{1 + \gamma \cos \chi}{(1 + \gamma^2 + 2\gamma \cos \chi)^{3/2}} .$$

In addition to these kinetmatic effects, account must be taken of systematic effects in the experimental apparatus. The actual reaction volume depends on the scattering angle. Therefore, the effective scattering pathlength must be known for all angles. To compute this accurately, the three-dimensional-primary beam intensity, slit geometry, and detection efficiency as a function of angle should be known. All of these cannot be determined in our case, but we can employ a valid approximation. The scattering pathlength is taken to be proportional to the area defined by the plane of intersection of the primary beam divergence and detector acceptance angle: this is illustrated in Fig. 6.

Finally, the counting statistics for detecting negative ions and fast neutrals are found to have a Poisson distribution. That is, the uncertainty in the number of counts is approximately the square root of that number.

Absolute Total Detachment Cross Section

To measure absolute total electron detachment cross sections the primary beam current I_o, detached electron current I_A and the pressure must be known accurately. The total cross section is determined by the equation:

$$\sigma = \frac{-1}{nL} \ln \left(1 - \frac{I_A}{I_o}\right)$$

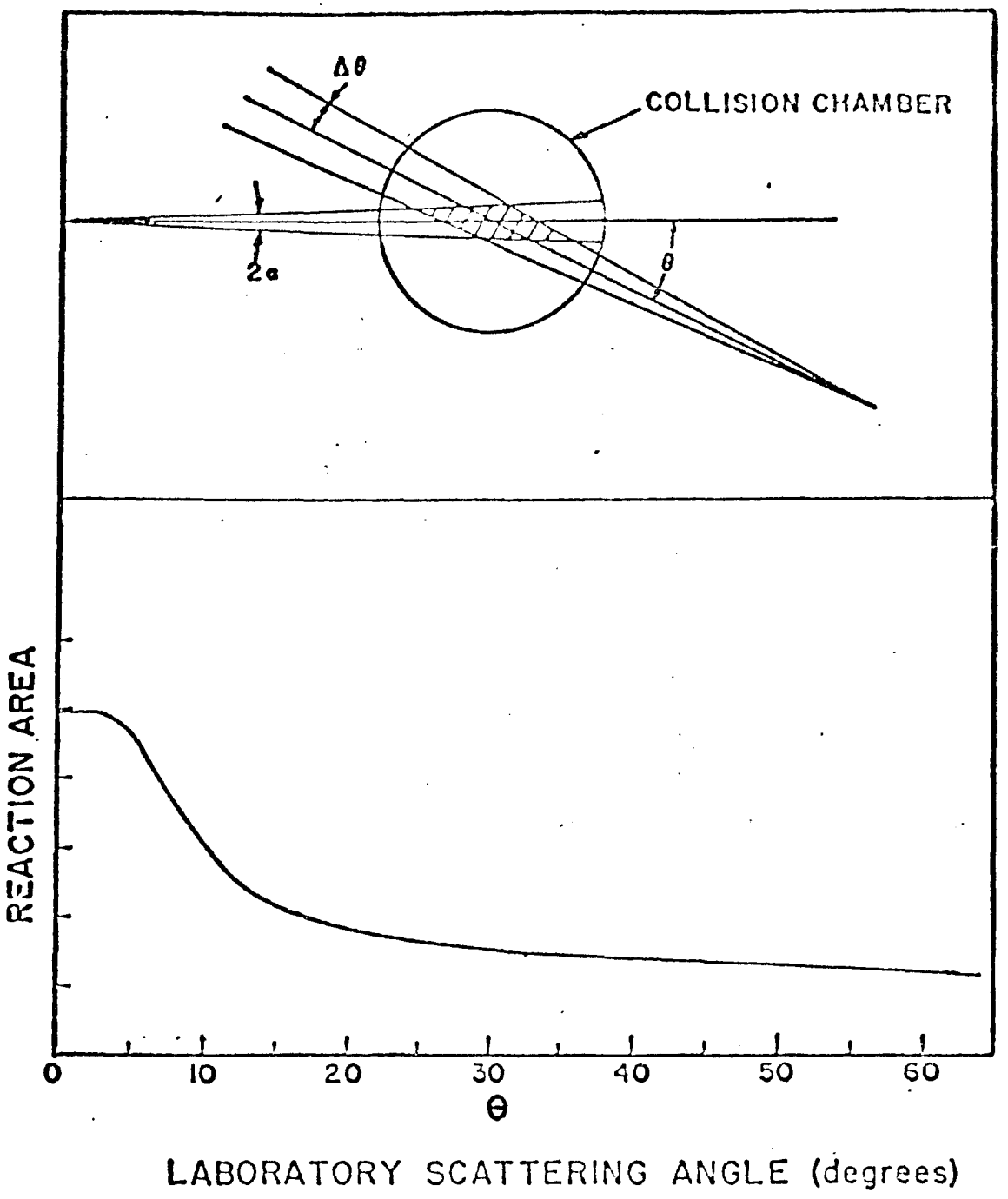
Δθ
COLLISION CHAMBER
2a
θ
REACTION AREA
0
10
20
30
40
50
60
θ
LABORATORY SCATTERING ANGLE (degrees)

Figure 6.

where n is the number of scattering centers per cubic centimeter and L is the scattering pathlength.

The detached electron current is collected on element A of Fig. 5. To insure that all of the detached electrons are collected on A a confining axial B field is combined with a slight negative voltage on grid II. Since some of the detached electrons travel twice through grid I before striking A, some may be attenuated by grid I. It was found that the electron current to A must be corrected by $2 \pm 2\%$ for this effect. Therefore, I_A of the above equation must be changed to $I_A = 1.02\ I_A'$, where I_A' is the measured quantity.

The axial B field is arranged so that the cyclotron radius of low energy electrons is less than the radius of element A at a field of 5 gauss. The guard ring which extends 0.050 inches beyond element A is kept at a slightly negative voltage ($\sim$0.1 volts) to repel electrons.

All of the aforementioned fields must be maintained so as to insure the most efficient detection of electrons without any systematic effects. For this reason, the B field is operated in a region where the detected current is independent of the magnitude of B.[19] Also the voltages on the guard ring and grid II are changed with primary beam energy to insure I_A remains independent of field strengths.

The primary beam current is determined by placing a large retarding voltage on grid I and measuring the current to element A and B with the same electrometer as is used to measure the detached current on element A. This procedure, therefore, minimizes any instrumental errors in determining the ratio I_A/I_o.

The capacitive manometer is connected by a small tube to the collision region. The membrane of the manometer is kept at a constant temperature of 322K. Thus, the effect of thermal transpiration must be taken into account when determining the pressure. In this case the diameter of the tube is much smaller than the mean free path of the target atoms, thus there is effusive flow through the tube. At equilibrium the flow of gas in and out of each region must remain constant and this leads to the condition $\frac{P_{cr}}{T_{cr}} = \frac{P_{mks}}{T_{mks}}$ [20] where the subscripts refer to the collision region and the MKS manometer in this equation relating the corresponding temperatures and pressures. The number density can be written as:

$$N = \frac{9.658 \times 10^{15}}{(300 \times 322)^{\frac{1}{2}}} \; P\left(\text{cm}^{-3}\right)$$

where P is expressed in units of 10^{-3} Torr and the denominator is a geometric temperature average which is a result of correcting for the thermal transpiration.

As mentioned earlier, the energy of the primary beam is determined by a retardation technique. In this procedure the ion current to element C is monitored as a function of the retarding voltage applied to grids I and II. (Grids I and II are shorted together to eliminate any electrostatic saddle points through which the ions could pass.) The derivative of the curve generated in this manner is approximately gaussian function the centroid of which is taken as the primary beam energy (refer to Fig. 4). A series of tests were done to ascertain any effect of surface contact potentials on the energy of the ion beam. A very liberal estimate would be that the laboratory energy is in error by no more than a quarter of an eV.[21]

With the uncertainties enumerated above it is believed the total detachment cross sections are accurate to $\pm$ 10% and by checks made at later dates reproducible to $\pm$ 6%.

III. THEORETICAL CONSIDERATIONS FOR NEGATIVE ION-ATOM SCATTERING

The possible reaction channels for collisions of negative ions with atoms are varied; there can be elastic scattering, direct electron detachment, charge transfer, excitation of the negative ion to auto-detaching states, and associative detachment. The experiments reported here focused on direct electron detachment and elastic scattering; the other channels will be discussed only in the context of how these channels may contribute to the experimental background when compared with direct electron detachment.

The chapter will be divided in two parts. In the first part, we wish to discuss the process of direct electron detachment in collisions of Cl^- with the rare gases and diatomic targets. The alkali target systems will be discussed separately in the second part of this chapter.

A. Direct Electron Detachment in Collisions of Negative Ions with Atoms

In collisions of Cl^- with the rare gases and diatomic targets we concerned ourselves primarily with direct electron detachment of the negative ion. A review follows of some relevant collision model calculations and *ab initio* potential calculations which will help us describe this collision channel.

Model Calculations for Direct Electron Detachment

Model calculations have been very useful in describing the collisional-induced electron detachment of negative ions. A few models will be reviewed including a local complex potential model which will be used to interpret the experimental results.

For very high incident energies ($E > 1$ KeV) a Born approximation can be applied to the scattering problem. Sida[22] used this approximation for the system H^- + He and was only able to achieve order of magnitude success in describing the electron detachment cross section. McDowell and Peach[23] had similar results for the H^- + H system.

Various other models extended the Born approximation. Lapontseva and Firsov[24] in a perturbation calculation used a delta function for an effective potential to describe detachment. The bound electron is treated as essentially free in the incoming and outgoing channels and the collision thus is equivalent to that of an electron elastically scattering from an inert gas atom, at a velocity equal to the relative velocity of the ion-atom interaction. Even at very high energies, this model did not predict the available experimental results and is obviously unsuited for any low energy description.

Demkov[25] has taken a different approach to describe the coupling to the neutral states. As the negative ion-atom interaction potential develops adiabatically the discrete state merges with a continuum of free electron neutral atom states. At this point, the ionization potential approaches zero and the wave function of the weakly bound electron appreciably overlaps regions where the effective potential is zero and detachment can occur. To model this effective potential at the crossing, a

time-dependent boundary condition is introduced for the electron wave function. This has the effect of providing a decay term for the electron-bound state at the crossing.

Devdariani[26] has evaluated the consequences of various forms of time-dependence and the model has been applied with limited success by Esalov et al.[27] to describe differential cross section measurements for H^- inert gas collisions.

Complex Potential Model

A local complex potential model has proven useful in describing collisional induced electron detachment studies previously investigated in this lab.[19,28,29] Lam[30] has compiled an excellent review and discussion of this formalism for both a classical model and the semiclassical treatment of Chen and Mizuno.[31] Here we simply wish to contrast the results of the classical and semiclassical models.

Since the de Broglie wavelength associated with the nuclear motion is short, some type of semiclassical approximation is appropriate, and we first derive a classical expression for the cross section following closely the development by Lam.[30]

It is assumed that the negative ion state and the neutral state cross at some internuclear separation (R_x). This curve crossing is schematically shown in Fig. 7. Following the potential curve of the quasi-molecule (AB^-) we see that at R_x the state crosses into a region where there is a continuum of possible outgoing states ($AB + e^-$). For collision energies greater than $V(R_x)$ this region is accessible and it is assumed

that we can ascribe an energy width $\Gamma(R)$ to the ionic state (AB^-). This width is inversely proportional to the lifetime of the anion state.

This probability for detachment can be described by introducing an imaginary part to the potential,

$$W(R) = V(R) - i/2\,\Gamma(R) \tag{1}$$

An imaginary potential in this form provides for a sink of elastically scattered products and thus will yield a survival probability term which modifies the usual elastic differential cross section.

Consider the time dependent wave equation for the nuclear motion:

$$\left[-\frac{h^2\nabla^2}{2\mu} + V(R) - i/2\,\Gamma(R)\right]\psi(R,t) = ih\frac{\partial\psi(R,t)}{\partial t}\,. \tag{2}$$

Multiplying the above equation by ψ^* and its complex conjugate by ψ, then subtracting, yields the continuity equation

$$\frac{\partial}{\partial t}\rho(R,t) + \vec{\nabla}\cdot\vec{j}(R,t) = -\frac{\Gamma(R)}{\hbar}\rho(R,t) \tag{3}$$

where ρ is the probability density and $\vec{j}$ is the probability current. We can rewrite the current as

$$\vec{j} = \rho\vec{v}\,.$$

The probability density can be constructed as a product of the elastic scattering probability density, ρ_o, times the survival probability, P, of the bound negative molecular state. Thus ρ is written as

$$\rho = \rho_o \cdot P$$

where ρ_o satisifes the homogeneous continuity equation.

$$\frac{\partial \rho_o}{\partial t} + \vec{\nabla} \cdot \rho_o \vec{V} = 0. \tag{4}$$

Now rewiritng Eq. 3 we have

$$\frac{\partial P}{\partial t} + \vec{V} \cdot \vec{\nabla} P = - \Gamma/\hbar \cdot P$$

or

$$\frac{dP}{dt} = - \Gamma/\hbar \cdot P \,, \tag{5}$$

from which we obtain

$$P_s = \exp\left[- \int_{-\infty}^{\infty} \frac{\Gamma}{\hbar} \, dt' \right]$$

With a change of variable the survival probability may be rewritten as:

$$P_s = \exp \left[- 2/\hbar \int_{R_o}^{\infty} \frac{\Gamma_{(R)}}{V_R} \, dR \right] \tag{6}$$

where R_o is the classical turning point for the real part of the potential and V_R is the radial velocity. This function depends on the impact parameter, through its dependence on the radial velocity. The differential cross section is then given by: $\sigma_{el}(\theta) = \sigma_o(\theta) \cdot P_s(\theta)$ where $\sigma_o(\theta)$ is in the usual form: $\sigma_o(\theta) = \frac{-bdb}{\sin\theta d\theta}$ (7) and θ is the deflection function which is a function of the impact parameter.

In the classical approach only the survival probability depends on the imaginary part of the potential; the deflection function has the usual form and dependence on the real part of the potential. This is not the case in the semiclassical development of Chen[31] in which the survival probability and deflection function depend on the imaginary part of the potential.

The formulation by Chen et al.[31] assumes again a complex potential, but the Schroedinger equation is solved for each partial wave by a JWKB approximation. Thus a complex phase shift, $\delta_l = \xi_l + i\eta_l$, is obtained which depends on both the real and imaginary parts of the potential. In this formalism the elastic differential cross section is given by:

$$\sigma(\theta) = P_s(\theta)\, b/\sin\theta \left| \frac{d\theta_{JWKB}}{db} \right| , \tag{8}$$

where the survival probability is:

$$P_s = \exp[-4\eta(b)]$$

and θ_{JWKB} is the deflection function which is defined in terms of wave number k, and impact parameter, $b = (l + \frac{1}{2})/k$ as

$$\theta_{JWKB} = \frac{2}{k} \frac{d\xi(b)}{db} .$$

Since the calculations presented will only be for total detachment cross sections, we now present a form for this function. In this model, the probability for detachment is negligible outside the crossing for the two states. Thus, we can construct the total detachment cross section by integrating the detachment probability over impact parameters from zero to a value corresponding to the crossing. The total detachment cross section can be written as: $\sigma_{det} = 2\pi \int_0^{b_x} [1 - P_s(b)]\, bdb$ (9)

where the detachment probability is $P = 1 - P_s$ and b_x is the impact parameter at which the turning point is equal to the crossing point. To determine the crossing impact parameter consider the radial velocity:

$$V_R = (2E/\mu)^{\frac{1}{2}} \cdot (1 - \frac{V(R)}{E} - b^2/R^2)^{\frac{1}{2}}. \tag{10}$$

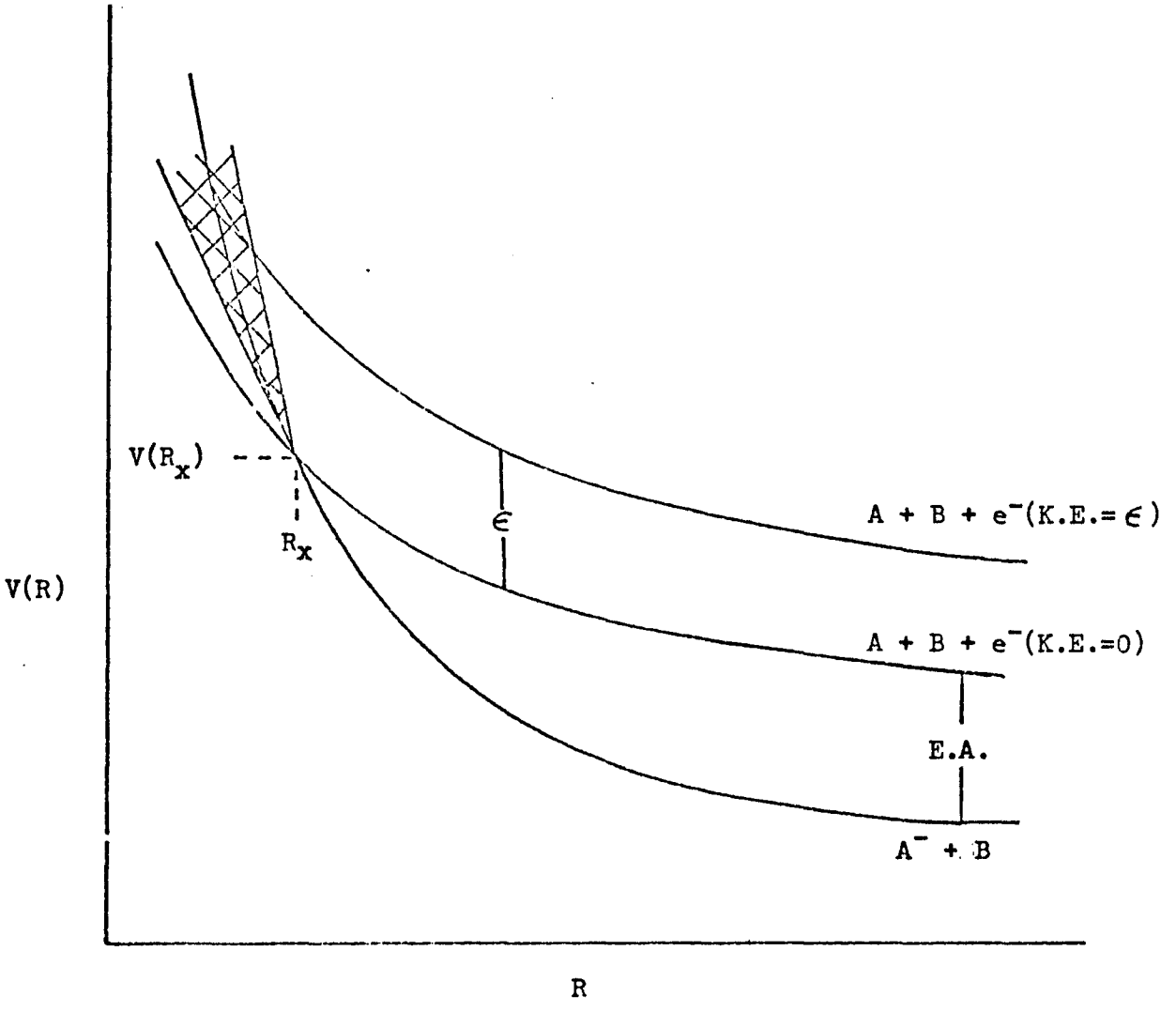

Figure 7. Schematic representation of the interaction potential for repulsive negative ion - atom states. The shaded region represents the decay width of the anion state as described in the text. Also shown is part of the continuum of free electron states.

If the turning point corresponds to the crossing, then $V_{R_x} = 0$ and we can solve for b_x:

$$b_x = R_x \left(1 - \frac{V(R_x)}{E}\right)^{\frac{1}{2}} \tag{11}$$

where E is the relative collision energy. The above form for the total detachment cross section will be used in calculations presented for the Cl^- + rare gas systems. The survival probability will be evaluated using the semi-classical formalism due to Chen and Mizuno.[31]

The width, $\Gamma(R)$, of the ionic state can be modeled by many functions. In the present work no attempt was made to find an optimum form for $\Gamma(R)$. We used a form suggested by O'Malley[32] which depends on the electron's asymptotic angular momentum:

$$\Gamma(R) \propto (R_x - R)^{L + \frac{1}{2}}, \quad R < R_x$$

where L is the angular momentum of the electron.

Some qualitative properties of the cross sections follow immediately from the complex potential model. The total detachment cross section should exhibit an energy threshold approximately equal to the value of the potential at the crossing, $V(R_x)$. The differential cross section would have a depletion of the elastic scattered signal at a threshold angle, corresponding to impact parameters which sample the region $R < R_x$. In both of these the sharpness of the threshold will depend on whether or not there is significant tunneling to the continuum for $R > R_x$.

Ab Initio Calculations for ArCl and $ArCl^-$

Olsen and Liu[33] have completed a self-consistent field (SCF) calculation for the adiabatic potentials, V(R), of the systems $ArCl^-$ and ArCl. The atomic basis sets for Ar, Cl and Cl^- were taken from the

tabulations of Clementi and Roetti,[34] with the Ar basis set augmented with optimized 4s, 4p and 3d functions of Saxon and Liu.[35] The SCF method does not yield accurate absolute values of the ionic and neutral potential curves and they have been corrected to give the proper energy separation at large internuclear distances. The above calculation showed the $X'\Sigma$ ($ArCl^-$) state crossing twice with the $X^2\Sigma$ (ArCl) state. The second or inner crossing was attributed by the authors to a correlation between $ArCl^-$ and the bound negative state or bromine in the united atom limit. Also the calculation showed the $A^2\Pi$ state of ArCl to be more repulsive than the $X'\Sigma$ ($ArCl^-$) state, which leads the authors to conclude that coupling between these states is insignificant.

The parameters which are of interest in this study are the outer crossing distance which is 3.45 a_o, and the value of the potential energy at the crossing, 10.1 eV above separated Cl^- + Ar. The authors point out that because of the relatively small basis set for the ArCl system the theoretical potentials may overestimate the energy at the crossing by 1-2 eV.

B. Collisions of Negative Ions with Alkali Atoms

Negative molecular ions of alkali-halides and alkali-hydrides have been investigated theoretically quite extensively in recent literature.[36-42] For these highly polar molecules, predictions can be made for the electron affinity (E.A.) of the molecule by noting a correlation between the E.A. and the dipole moment.

An initial model then for these systems is that of an electron in the field of a dipole. We will proceed with a review of a solution of this simple model followed by a report on the ab initio potential calculations for the systems NaH^- and $NaCl^-$.

The Schroedinger equation for an electron in the field of a finite dipole is rigorously soluble and has been investigated in detail by Wallis et al.[43] They were able to determine the eigenfunctions and energies for a given charge separation of the finite dipole. The eigenfunctions are determined by separation of variables, and for a given symmetry, there is an infinity of bound states. As the fixed charges are brought closer together, the bound states will vanish and there will be a critical separation which will just be bound. Wallis and his coworkers[43] were not able to determine this critical dipole moment.

Wrightman[44] made the earliest known calculation of the minimum separation for binding, .639 a_o. Mittleman and Myerscough[45] examined the solutions to the Schroedinger equation for the case where the total energy of the bound electron approaches zero. They performed a perturbation claculation for small changes in the charge separation. The critical dipole moment for binding was found to be:

$$\mu_c > 1.625D \text{ (D = Debye = } 10^{-8} \text{e.s.u.-cm)}$$

Using a different approach, Turner and Fox[46] arrived at the same critical value.

Crawford[47] has made a general study of bound states of an electron in various dipole-like fields. A calculation of the zero energy solutions of a finite dipole yields a set of critical dipole moments

corresponding to different symmetries of the wave functions, again: $\mu_c > 1.625$D. These results are also applicable to an electron in the field of a point dipole with a repulsive central core.

The next logical step is to extend the above to the study of real polar molecules. Crawford[48] has examined this problem and drawn some conclusions when including electronic, vibrational and rotational motion in negative molecular ions. Beginning with a properly antisymmeterized wave function, Crawford[48] showed that for a molecule with its nuclei fixed and $\mu \geq \mu_c$ there exist an infinite number of discrete negative ion electronic states. This result followed from simply noting the general eigenvalue behavior of the Schroedinger equation with the proper form of the wave function. When vibration is included, if the average dipole moment does not fall below μ_c the elctron still has an infinite number of bound states.

When including rotational motion of the molecule, it is difficult to make predictions using generalized wave functions in the Scroedinger equation. Crawford[48] used a rigid rotor model of a dipole and found that at most the critical dipole moment for binding rises to 2D and most surely there is binding for $\mu > 2.5$D.

As listed in Table 1 the dipole moments of the reactants studied are all greater than six debye and should support bound negative molecular states.

Carlsten, Peterson and Lineberger[49] have given direct experimental evidence for a bound state of $LiCl^-$. Their determination gives an electron affinity which is an order of magnitude below that predicted

for an electron in a simple finite dipole field. This result is not surprising since the pure dipole field does not consider the effects of core repulsion or finite atomic sizes which are important at small internuclear separations.

Ab Initio Potential Calculations

Simons[41] has compiled an extensive review of recent theoretical studies of negative molecular ions. Ab initio potential calculations have been completed by Jordan and Wendoloski[39] on the system $NaCl^-$ and NaH^- and Karo, Gardner and Hiskes[42] have investigated the NaH^- potential energy curves. Here we wish to report on the calculations which will be employed in the later chapter to interpret experimental results.

For the systems NaH^- and $NaCl^-$, Jordan and Wendoloski[39] employed a Hartree-Fock (HF) method to solve for the E.A. of the bound electron. In this approximation a HF calculation is made for the neutral molecule and the anion. By noting the vertical separation between these potential curves the electron affinity of the anion can be deduced. A conventional HF self-consistent field calculation for NaH^- was done by KGH[42] using a linear combination of atomic and molecular orbitals for the ground eigenstates of the neutral molecule and the negative ion. The two states appear to cross at 2.6 a_o at a value of the interaction potential which is less than zero.

The results of these ab initio calculations will be employed in an analysis of our experiments. The potentials will be fit to convenient analytical forms to facilitate the integrations. Listed in Table 3 are the equilibrium separations and potential well depths for these calculations.

IV. ABSOLUTE TOTAL DETACHMENT CROSS SECTIONS FOR Cl^- ON He, Ne, Ar AND Kr

Absolute total detachment cross section measurements were made for the systems Cl^- + He, Ne, Ar and Kr for relative energies ranging from around threshold for detachment to approximately 150 eV. Attention was focused primarily on the threshold for direct electron detachment, which is the most important inelastic channel at these low energies.

These reactants have been investigated previously, and we wish first review earlier total and differential cross section measurements. Following this review we will discuss broadening effects in the experimental data, and then present the results and analyses of the present measurements.

Related Cross Section Measurements

The earliest reported measurements for these systems were elastic differential and charge exchange cross sections for negative ions of chlorine and bromine with various gaseous targets. These experiments were completed by Rosenbaum[50] over an energy range of 1-4 KeV.

Bydin and Dukel'skii[51] reported total detachment cross sections for negative halide ions colliding with the rare gases and H_2 over an ion energy range of 0.2-2 KeV.

Integral cross sections for elastic scattering of Cl^- from the rare gases were determined by Boerboom, Van Dop, and Los[52] in the energy range of .15-4 KeV. They deduced the interaction potential for various potential models for their experimental results.

The energy spectrum of the detached electrons for collisions of halide negative ions with the rare gases was determined by Bydin.[53] He found that at energies above 500 eV, the energy spectra of the detached electrons showed a maximum around 1-2 eV with another maximum at 6-7 eV which was attributed to auto-detaching states. The latter peak became significant at higher collision energies.

Fayeton et al.[54] have studied both electron detachment and inelastic processes in collisions of Cl^- with the rare gases. These studies were carried out over a laboratory energy range of 80-2000 eV. For their low energy experiments they had success in applying a complex model with potential parameters which had been determined experimentally by Champion and Doverspike[19] for the same systems.

The results reported here are an extension of the experiments of Champion and Doverspike[19] in which the relative differential and absolute cross sections for Cl^- colliding with the rare gases were measured. By using a semiclassical complex potential model, they were able to deduce reasonable local complex potentials which yielded calculated cross sections in satisfactory agreement with experimental results. In these total cross section experiments the threshold region was difficult to examine in detail because of low beam intensities and the rather large energy spread in the primary ion beam.

Threshold Behavior

The systems presented here all exhibit the same behavior: the cross section rises rapidly from the energy threshold (which is approximately twice the electron affinity of the halogen) to a near constant value, if the relative energy is sufficiently high. Our main interest lies in the threshold region and corrections must be made for effects which cause the true detachment cross section to be broadened.

These are three possible sources of this broadening (1) thermal motion of the target gas, (2) energy spread of the primary ion beam, and (3) the existence of stable isotopes in either the primary ion beam or target gas. Of these three the most important is (1) which has been discussed in detail by Chantry.[55] If the true detachment cross section is $\sigma_{true}(E)$, where E is the relative energy, then the observed cross section is a result of the convolution:

$$\sigma_{obs}(E) = \int G(E' - E)\, \sigma_{true}(E')\, dE'$$

where $G(E' - E)$ is an appropriate apparatus function. If $E \gg kT$, then the broadening function due to thermal motion can be represented by a gaussian function with a full-width-half-maximum given by[55]

$$W_1 = (11.1 \cdot \gamma \cdot kT \cdot E)^{\frac{1}{2}}$$

where γ is the ratio of the projectile mass to the total mass, T is the temperature of the target gas, and E is taken as the threshold energy.

The laboratory energy spread of the primary ion beam is ~ 0.60 eV, FWHM, and when converted into the C.M. frame of reference gives the width of the second source of the convolution.

The third source of broadening is due to the existence of isotopes in the reactants, which causes the mapping of the laboratory data into the C.M. frame of reference to be non-unique. For instance the Wien filter cannot resolve the two isotopes of chlorine, Cl^{35} and Cl^{37}, so that the average mass (35.5 amu) is used in computing the center of mass energy. This isotope effect, however, is rather small and for systems reported here, could cause broadening with a characteristic width $W_3 = 0.15$ eV.

The total convolution function is taken to be a gaussian function with a width of

$$W = (W_1^2 + W_2^2 + W_3^2)^{\frac{1}{2}}$$

where the subscripts refer to the source of broadening. The widths associated with the various reactants are given in Table 2.

To deconvolute the experimental results, a method which uses an iterative technique to solve for $\sigma_{true}(E')$ in the integral equation was used. This procedure developed by Ioup[56] requires uniformly spaced experimental data, which in our case was not available. To generate an equally spaced array from the experimental data, a standard numerical interpolation scheme (Lagrange-Aitken) was used.

To test the deconvolution scheme and the magnitude of the effects of thermal broadening, we have used a simple analytic function to represent the cross section. The form of the function chosen is that of a charging capacitor which switches on at $E_{th} = 9$ eV:

$$\begin{aligned} \sigma(E') &= 0 && E' \leq E_{th} \\ \sigma(E') &= 10 \cdot \left\{1 - \exp\left[-A(E' - E_{th})\right]\right\}, && E' > E_{th} \end{aligned} \tag{12}$$

In this form the convolution integral can be performed exactly (Eq. 37 of Ref. 55) and the results of the convolution, with W_1 = 1.26 eV, are shown in Fig. 7(b). It is clear that the inclusion of thermal broadening will cause $\sigma_{obs}(E)$ to differ from $\sigma_{true}(E)$ only in the region near threshold, but in that region, the effects will be important and their neglect could lead to a slight underestimation of E_{th}. This point has been discussed by Chantry.[55]

The numerical deconvolution was applied to the results of the exact convolution and, as can be seen in Fig. 7(b), the results are good in that the original function $\sigma(E)$ is recovered.

The threshold region for the reactants, Cl^- + Ne, is shown in Fig. 8(a). The experimental results are given along with a deconvolution and a complex potential calculation using the potential parameters obtained by Champion and Doverspike.[19] As can be seen, agreement between the calculated and deconvoluted results is excellent.

The total detachment cross section in the threshold region is shown for the Cl^- + He system in Fig. 9. Both the experimental results and deconvolution are presented; as in the previous case, the threshold for detachment is approximately twice the electron affinity of chlorine.

The results for the systems Cl^- + Ar, Kr are shown in Fig. 10(a). This cross section does not appear to approach zero at the electron affinity of chlorine, but remains finite for $E < E.A.$ For these reactants of light projectiles on heavy targets, elastic backscattering in the laboratory reference frame is possible and this can contribute to an apparent cross section $Q_A(E)$, which is the sum of the detachment cross section and the backscattering contribution:

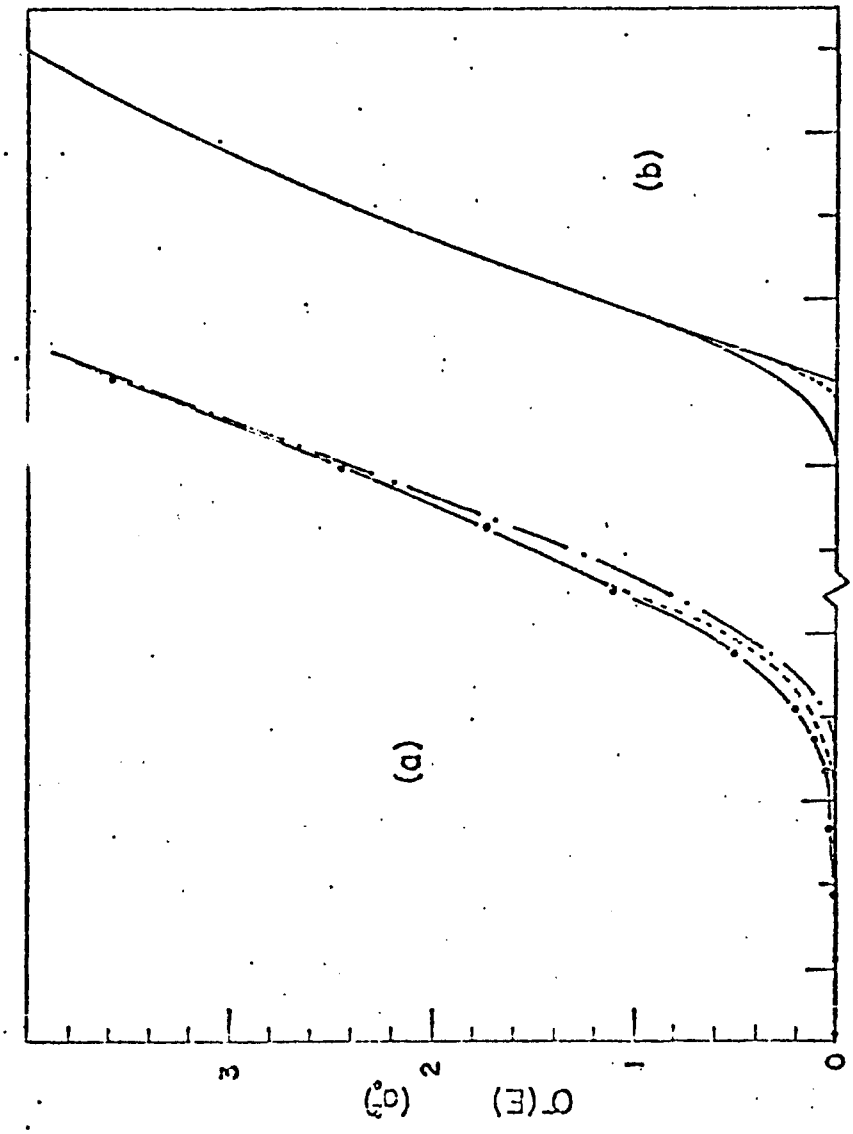

Figure 8. (a): $\sigma(E)$ for Cl^- + Ne -- the solid dots are the experimental measurements and the dashed line is the result of deconvoluting these data. The dot-dash line is a complex potential calculation for Cl^- + Ne from Ref. 19. (b): An assumed cross section form given by Eq. 12 and its exact convolution. The dashed line is the result of a numerical deconvolution.

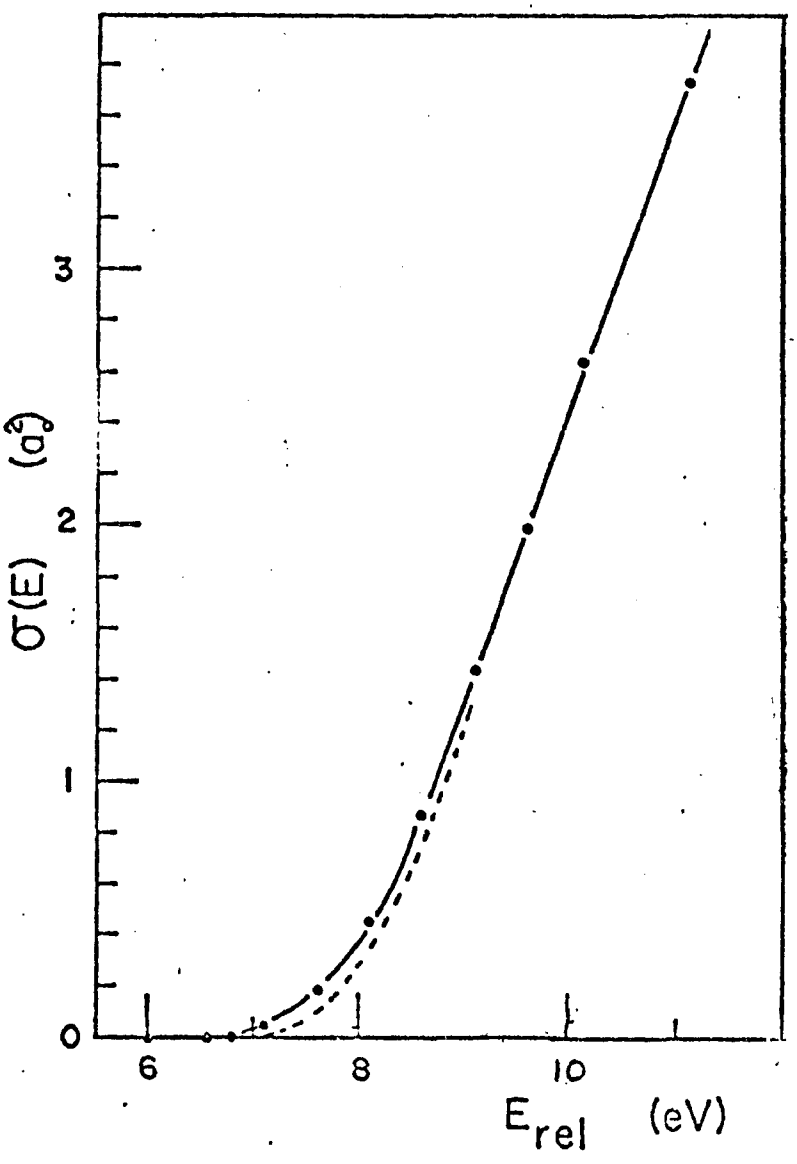

Figure 9. $\sigma(E)$ for Cl^- + He.

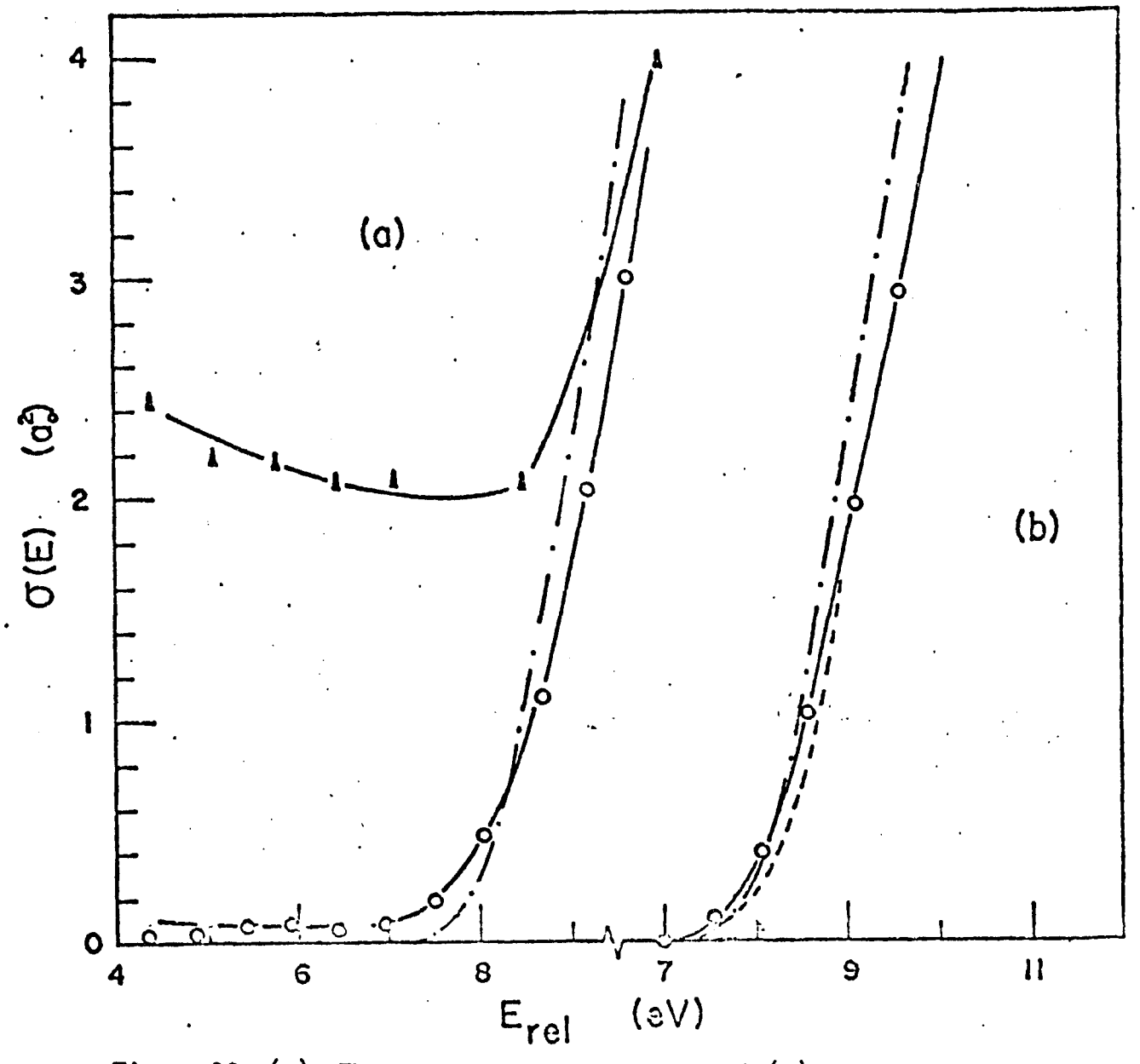

Figure 10. (a): The apparent cross section, $Q_A(E)$, as discussed in **text.** Triangles - Cl^- + Kr; open circles - Cl^- + Ar. (b): Corrected **detachment** cross section which results from subtracting the **estimated** backscattering contribution from the data given in (a). **The** dashed line is the result of deconvolution. The dot-dash line **is a** complex potential calculation for Cl^- + Ar, Kr from Ref. 19.

$$Q_A(E) = \sigma(E) + Q_{BS}(E)$$

Based upon the experimental results for the previous reactants, it is reasonable to assume that $\sigma(E)$ is approximately zero for $E \lesssim 7.5$ eV and that for this energy range $Q_A(E) \approx Q_{BS}(E)$.

Potential parameters exist for both Cl^- + Ar and Kr,[19] so that the elastic backscattering contribution can be calculated as follows. Referring to Fig. 5, let us define the Z-direction as that of the primary ion beam with Z = 0 defining the plane of the circular element labled A. The elastic backscattering contribution is then given by:

$$Q_{BS}(E) = \frac{\pi}{(L - Z_o)} \int_{Z_o}^{L} b_o^2(E_1, Z)\, dZ$$

where L is the total scattering pathlength, Z_o is the amount by which the guard ring extends beyond Z = 0, and $b_o(Z)$ is determined from the real part of the potential by

$$b_o(E_1, Z) \leftarrow \Theta_{cm}(E_1, Z) \leftarrow \Theta_{lab} \leftarrow \tan^{-1}\left(\frac{-R_A}{Z}\right)$$

where R_A is the radius of element A.

For the energy range from 4 eV to 8 eV, $Q_{BS}(E)$, as calculated above, is found to be approximately constant at $Q_{BS}(E) = 0.10\ a_o^2$ which is in excellent agreement with the experimental observations for Cl^- + Ar. In the case of Cl^- + Kr, $Q_{BS}(E)$ is calculated to be $Q_{BS}(5\text{ eV}) = 2.1\ a_o^2$ and $Q_{BS}(7\text{ eV}) = 1.9\ a_o^2$, which is also in good agreement with the experimental results. Therefore, it is reasonable to assume that for these reactants, the negative current measured on element A is due entirely to elastic backscattering for collision energies below 7.5 eV.

We have corrected the Cl^- + Ar data for the effects of elastic backscattering and show the correction and deconvolution in Fig. 10(b); because the effect was so large for the Cl^- + Kr reactants no attempt was made to correct the experimental results. Also shown is a calculation for Cl^- + Ar and Kr which in this region is the same for both reactants. The agreement of the calculations with the experimental results is good.

In chapter III we reported the results of an ab initio calculation of Olsen and Liu[33] for the potential energy curves of $ArCl^-$ and ArCl. They found that the states cross at an internuclear separation of R_x = 3.45 a_o which agrees well with an experimental determination by Champion and Doverspike[19] of R_x = 3.39 a_o. This crossing occurs at an ab initio interaction potential energy of $V(R_x)$ = 10 eV. Based upon the premise that the coupling of the ionic state to the neutral state should be quite small for $R > 3.45\ a_o$, this crossing energy would appear to be about 2½ eV higher than that indicated by the experimental results of Fig. 10(b).

The complete experimental results are displayed in Fig. 11 for Cl^- + He, Ne, Ar and Kr. Corrections for broadening are not observable on such a scale and are not included. The cross sections for Cl^- + Ne, Ar and Kr differ by 3% to 8% in the energy range $E > 50$ eV from the values reported earlier.[19] The cause of this discrepancy is unclear, but it may be due in part to the determination of the scattering gas pressure.[57]

A comparison of the cross section for Cl^- + He with the results of Bydin and Dukel'skii[51] shows the present cross section approximately 18% lower for a relative energy of 14 eV. For Ne, Ar and Kr, a reasonable

extrapolation of the present results lies 32-38% lower than those of Bydin and Dukel'skii.[51]

In summary, we have found that the onset of detachment has an energy threshold of approximately twice the E.A. of chlorine. Moreover, a complex potential model calculation gives a satisfactory description of the experimental observations.

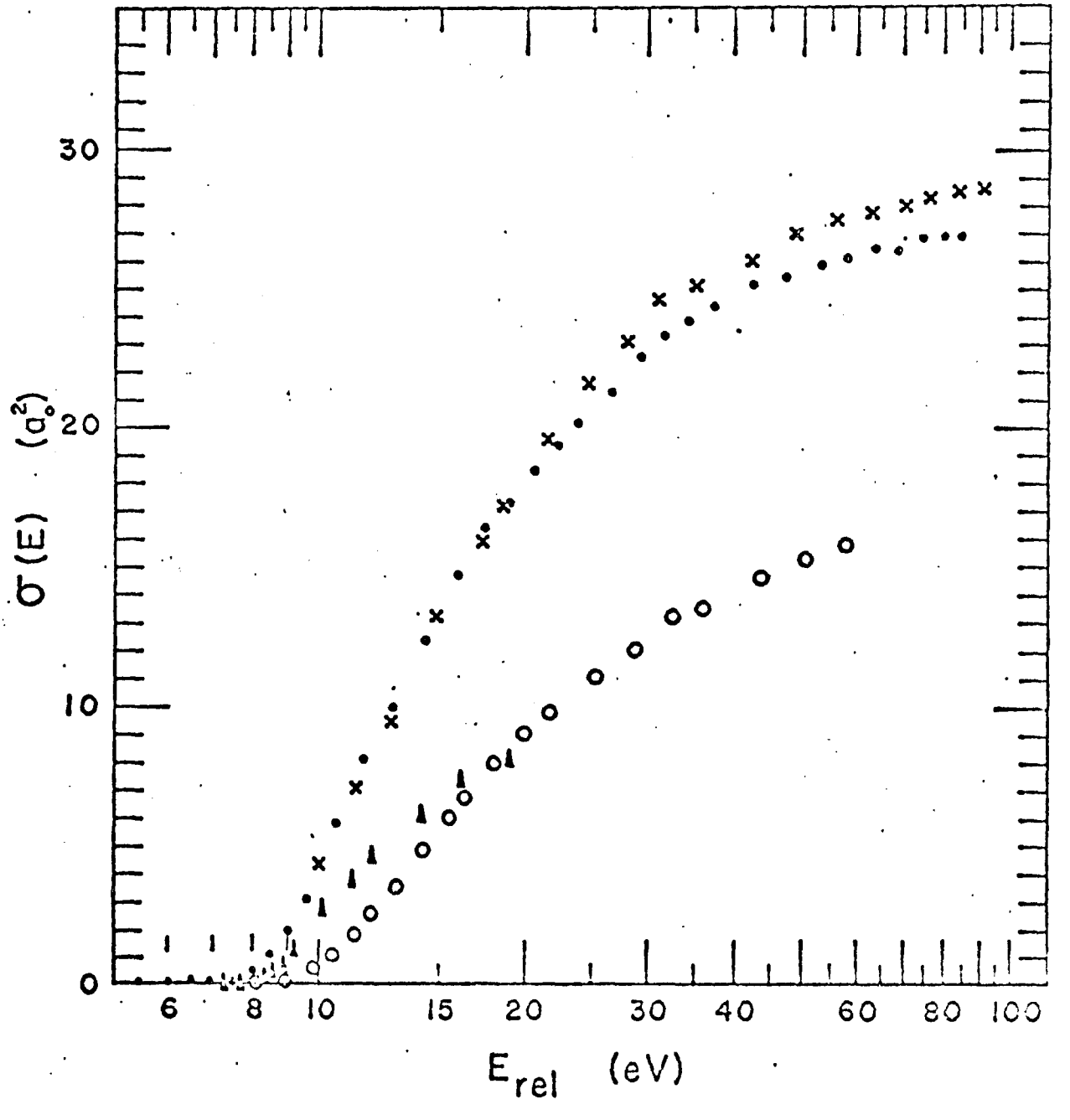

Figure 11. $\sigma(E)$ for Cl^- + He (triangles), Ne (open circles), Ar (solid dots) and Kr (crosses).

V. ELECTRON DETACHMENT IN COLLISIONS OF Cl^- WITH VARIOUS MOLECULAR SPECIES

Absolute total detachment cross sections have been measured for relative collision energies in the range from around threshold to approximately 150 eV for collisions of Cl^- with H_2, D_2, O_2, N_2, CO and CO_2. Relative elastic differential cross section measurements were made for the reactants Cl^- + N_2, CO and CO_2. In addition, we have also measured the relative differential cross sections for "fast" Cl atoms produced in the detachment process for the systems Cl^- + O_2, N_2, CO and CO_2.

The potential surfaces for these systems are at the present time unavailable, thus only a qualitative analysis of the experimental observations will be given. The total cross sections will be presented first, followed by the relative elastic and inelastic cross sections.

A. Absolute Total Detachment Cross Sections

Absolute total detachment cross sections have been determined and the measurements and their deconvolutions are presented in Figs. 12-17. The deconvolution scheme is the same as that used in the analysis of the Cl^- and rare gas experiments.

The threshold region for the systems Cl^- + H_2 and D_2 are shown in Figs. 12 and 13. Again, as in the case of the rare gas targets, the energy threshold for detachment is well above the E.A. of chlorine. A comparison with the results of Bydin and Dukel'skii[51] at 8.8 eV shows

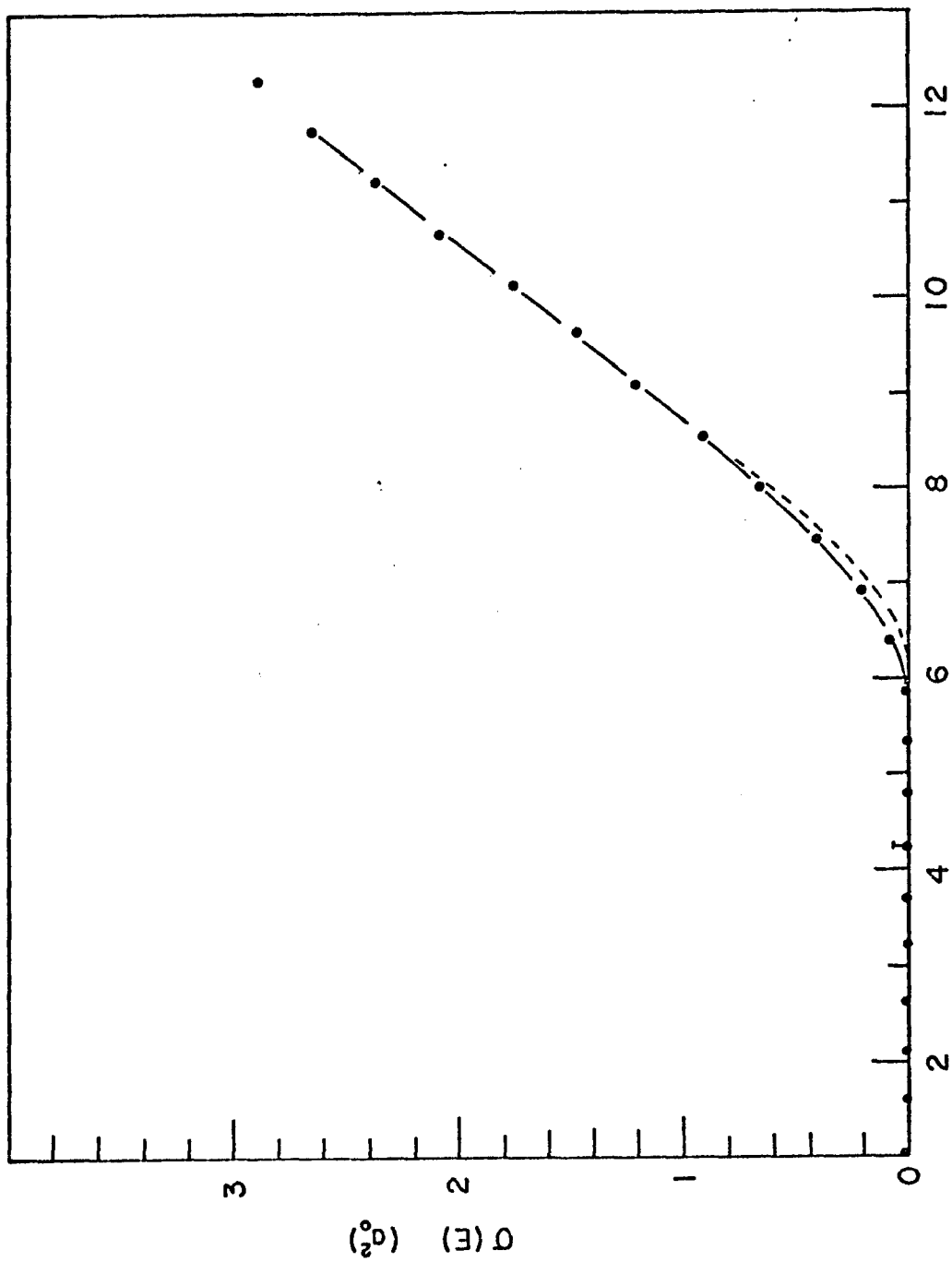

Figure 12. $\sigma(E)$ for $Cl^- + H_2$. The solid dots are the experimental measurements and the dashed line is the result of deconvoluting these data.

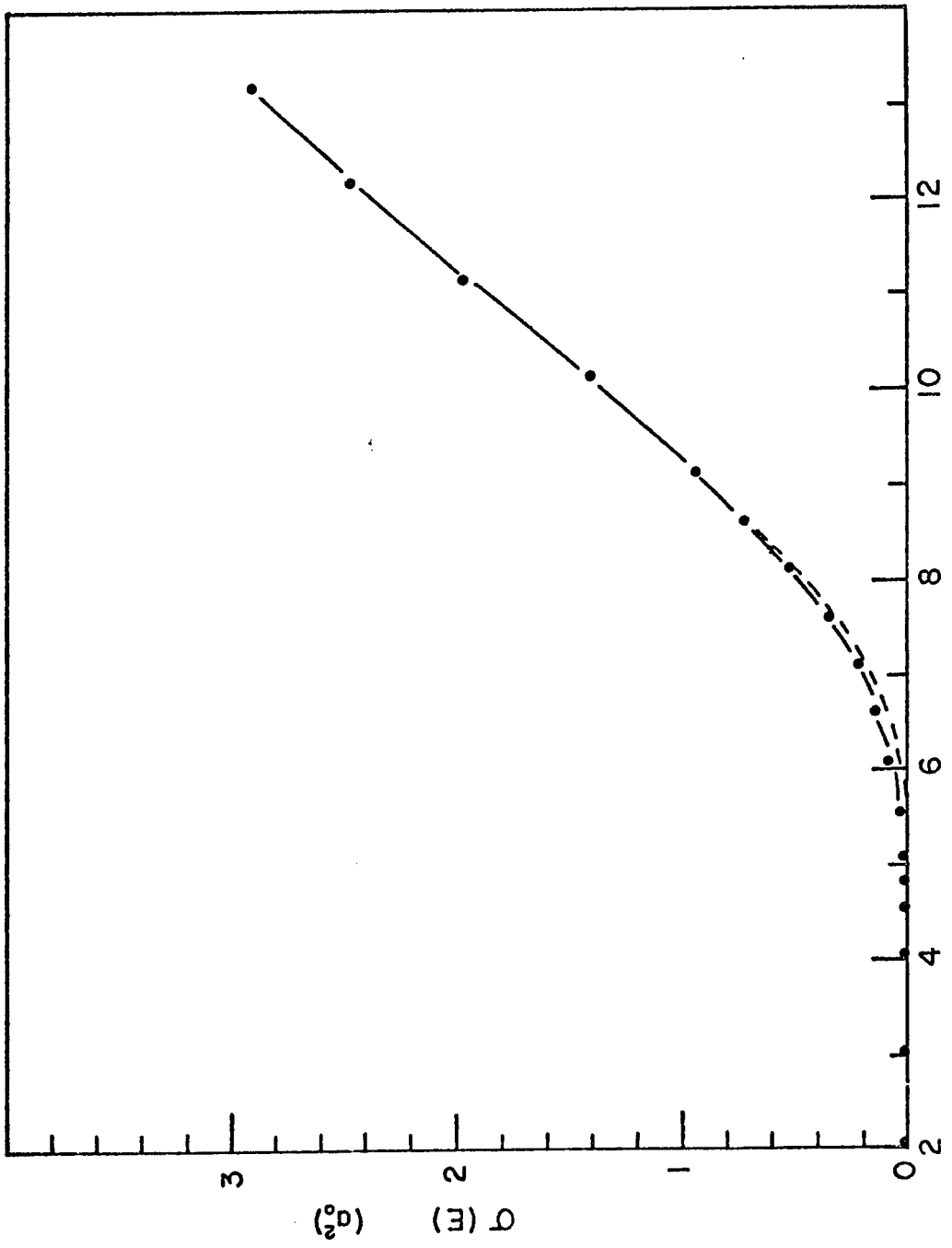

Figure 13. $\sigma(E)$ for $Cl^- + D_2$. The solid dots are the experimental measurements and the dashed line is the result of deconvoluting this data.

that our results are approximately 60% below their results for the H_2 target.

A close inspection of Figs. 12-13 reveals that, for a given relative energy, the cross section for H_2 lies slightly above that of D_2. This is in direct opposition to the predictions of a local complex potential model if we assume that the potential surfaces are the same for the reactants. The complex potential model predicts an isotope effect which can readily be understood by considering the classical form of the survival probability which is a function of the collision velocity. At the same relative energy the heavier isotopic system will have a slower relative velocity and thus a longer collision time. Therefore, the system $Cl^- + D_2$ will have a larger probability for detachment since it spends more time in the region where detachment is energetically possible. One would expect the cross section of D_2 to be above that of H_2 but that was not the case. Champion et al.[58] have studied this isotope effect for H^- and D^- colliding with various targets and found the results could not always be explained by a model using a local complex potential. (It should be noted, however, that these arguments ignore the difference in the rotation and vibration of these molecules, and also they ignore the fact that the potentials are not spherically symmetric.)

For all of these molecular targets there are other channels which could lead to an apparent signal for electron detachment such as dissociative charge transfer, charge transfer, or rearrangement. The first two channels could result in thermal energy negative ions that could be collected on element A and interpreted as detached electron current.

The cross sections for these rearrangement processes are largely unknown for these reactants. Cheung and Datz[2] found evidence of other detachment channels in collisions of Cl^- with H_2 at laboratory energies above 500 eV. In a similar experiment for Cl^- on O_2 they only detected the simple detachment channel.

The experimental results in Fig. 15 for the system Cl^- and O_2 show the detachment cross section rising slowly with decreasing energy below the predominant threshold at 4.5 eV to a value of 0.2 a_o^2 at 1 eV. This value (0.2 a_o^2) is in agreement with the cross section for charge transfer as measured by Vogt and Opiela[60] in this energy range. This charge transfer cross section will contribute to the background in the measurement of the cross section for direct electron detachment. Also, the process of associative detachment, $Cl^- + O_2 \rightarrow ClO_2 + e^-$, may contribute to the background below 4.5 eV.

The results of the measurements for the detachment cross sections for $Cl^- + N_2$ and CO around threshold are shown in Figs. 15 and 16 and the cross sections are seen to continue smoothly to zero. The detachment cross section for $Cl^- + CO_2$ around threshold is shown in Fig. 17. This system exhibits the same behavior as the reactants Cl^- + Ar(Kr; that is for these light projectiles on heavy targets elastic backscattering in the laboratory leads to an apparent cross section below the predominant threshold. We can assume that the cross section below 9 eV is due to this backscattering effect.

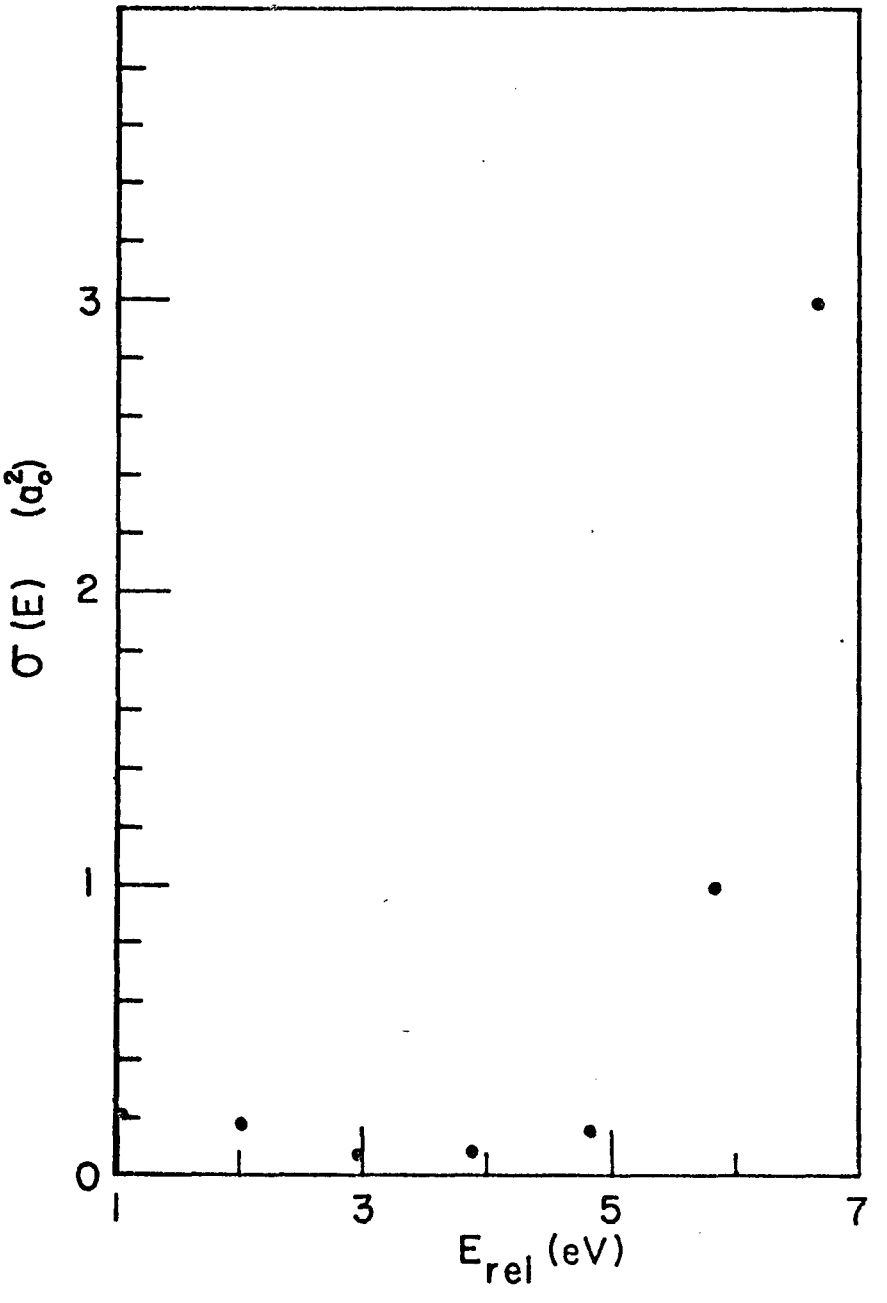

Figure 14. $\sigma(E)$ for $Cl^- + O_2$.

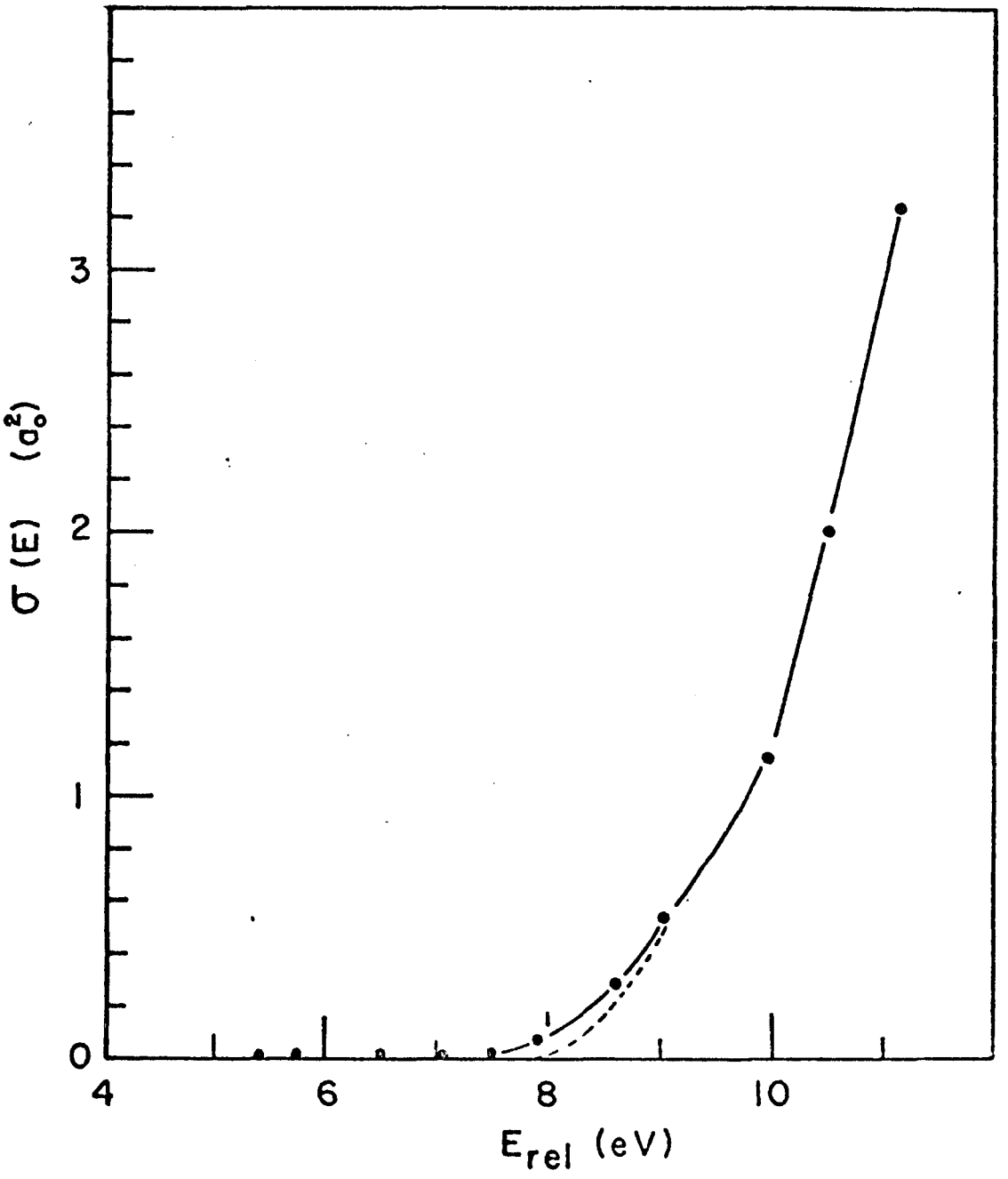

Figure 15. $\sigma(E)$ for $Cl^- + N_2$. The dashed line is the result of a deconvolution.

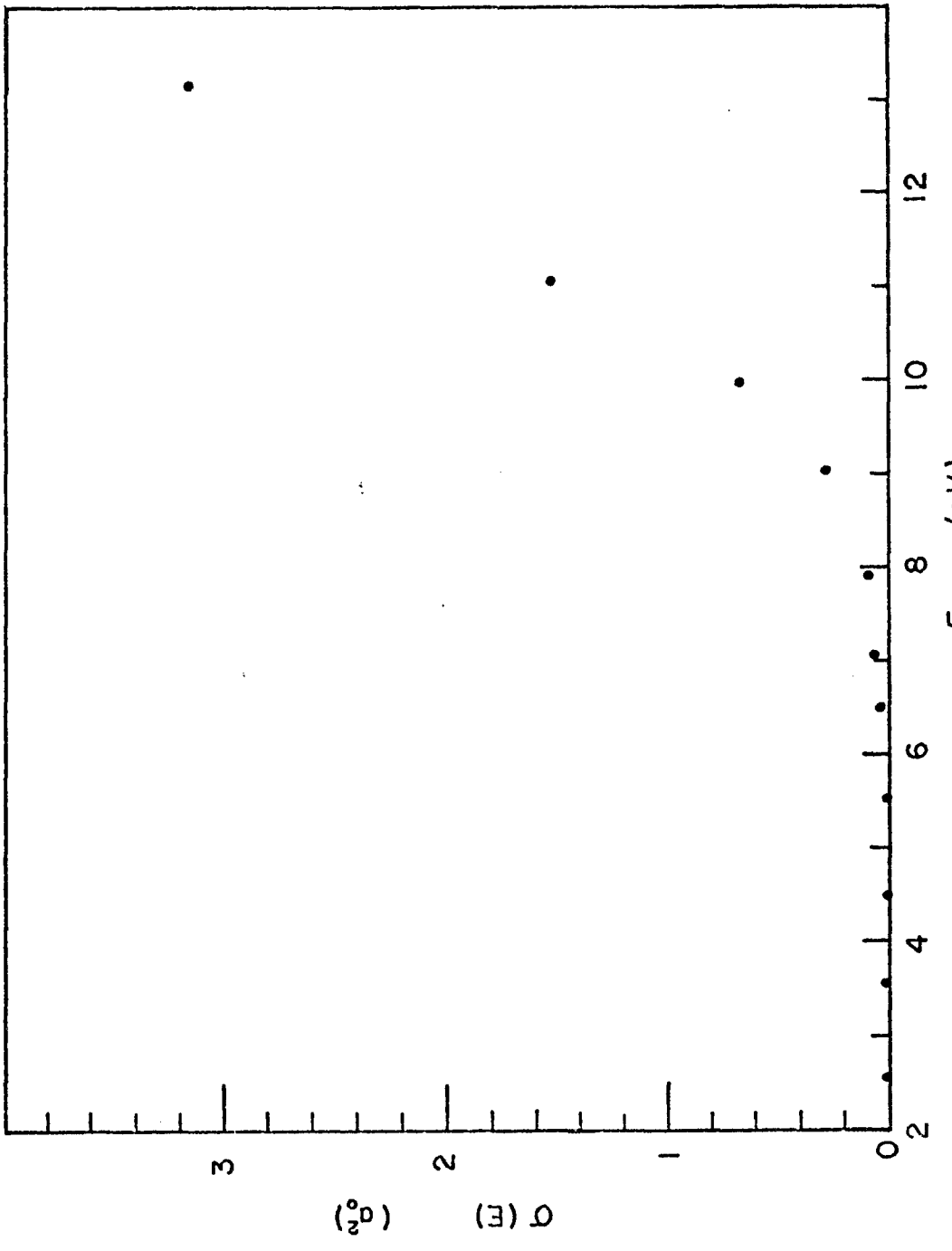

Figure 16. $\sigma(E)$ for Cl^- + CO.

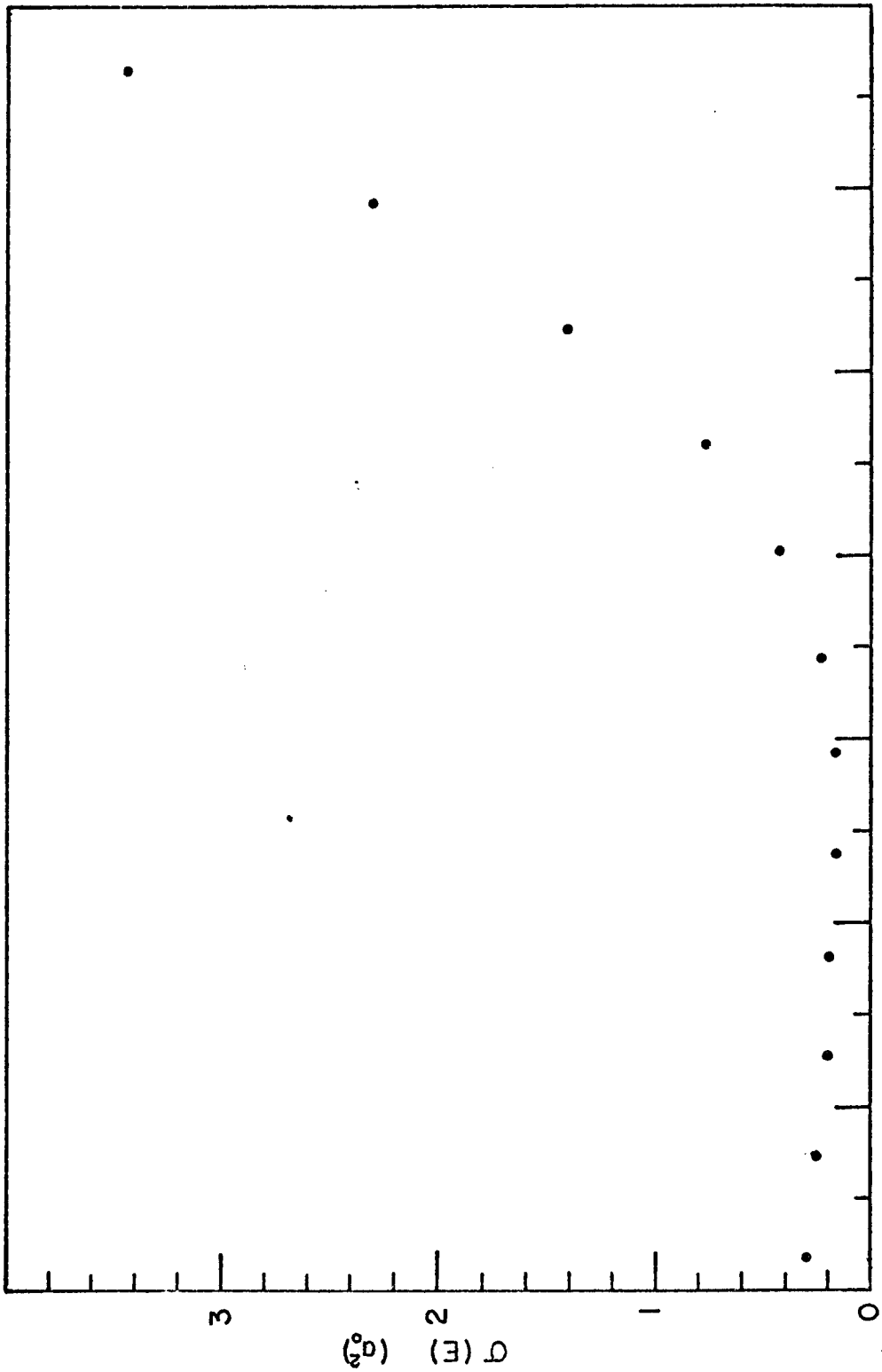

Figure 17. $\sigma(E)$ for $Cl^- + CO_2$.

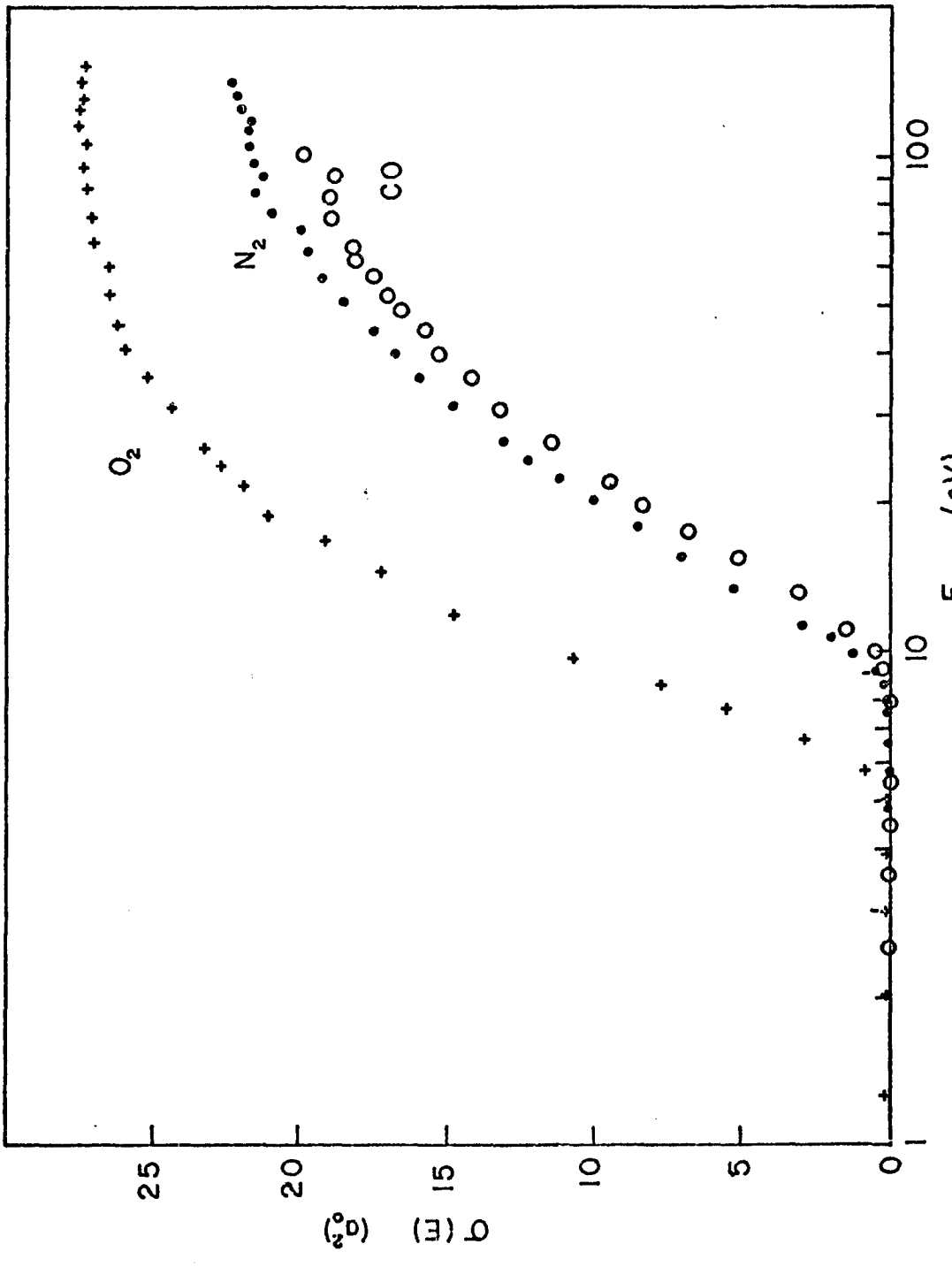

Figure 18. σ(E) for $Cl^- + O_2$, N_2, CO

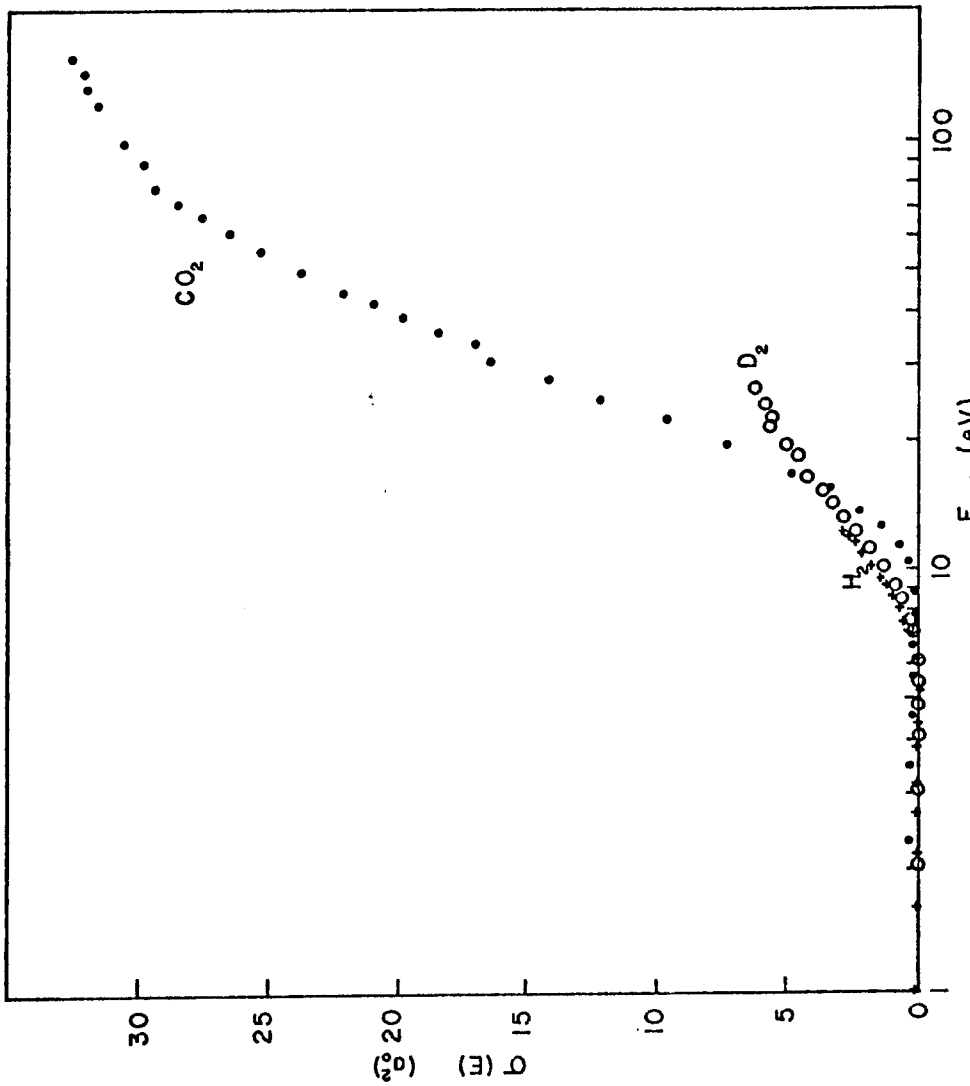

Figure 19. $\sigma(E)$ for $Cl^- + CO_2$, D_2, H_2

In Figs. 18-19 the cross sections are shown over the entire energy range sampled for all molecular targets. Dimov and Rosylakov[61] have measured the total detachment cross section for the O_2 and CO_2 systems at laboratory energies above 225 eV; when compared with our results they are found to lie 25% and 13% lower respectively.

B. Relative Differential Cross Sections

Relative differential cross sections for the scattering of Cl^- by N_2, O_2, CO and CO_2 as well as the relative differential cross sections of the fast (neutral) chlorine atoms produced in collisions of Cl^- with these molecular targets have been measured for laboratory collision energies in the range 50-260 eV. Selected examples of these measurements are shown in Figs. 20-24. The elastic results are plotted as usual in center of mass coordinates, while we have chosen to display the neutral differential cross sections as functions of the reduced coordinate $\gamma = E_1 \cdot \theta_1$, where E_1 is the laboratory collision energy and θ_1 the laboratory scattering angle. Over the energy and angular range of the present experiments, γ never differs by more than 2.7% from the corresponding center of mass γ-values for all the scattering systems considered here. It is well known that the quantity γ is primarily a function of the impact parameter for small-angle forward scattering.[69] Thus, any features in the scattering that occur at the same value of for different collision energies indicate that they are due to the same region of the interaction potential.

In chapter II we have discussed the neutral particle detector efficiency as a function of energy. If a single endothermic process is responsible for the detachment of electrons, then the scattered neutrals will have a decreasing kinetic energy with increasing angle. However, at the energies reported and for the range of scattering angles investigated the change of kinetic energy of the scattered neutrals is at most a few percent and will not appreciately affect the overall shape of the measured differential cross section.

The cross sections for neutral production by the targets N_2, O_2 and CO_2 all show the same basic structure. One common feature is a relatively small peak at χ = 0 which is spurious. Due to detachment on slits etc., a large neutral signal is observed at zero degrees with no target gas present: this signal has been subtracted from the "gas-in" measurements. However, subtraction of this background signal still leaves a non-zero signal around χ = 0, because reactions occuring in the immediate vicinity outside the defining slits of the collision region give an additional unwanted signal with target gas present.

For N_2, O_2 and CO_2 target gases, the measured neutral cross sections rise rapidly at small χ-values, reach a prominent maximum, then decrease more slowly with increasing χ. The maximum in the CO_2 cross section occurs at a characteristic value of χ in the neighborhood of 1100 eV-deg, which is essentially independent of collision energy. However, the maximum in the O_2 cross section shifts to larger values with increasing collision energy. There appears to be a slight trend in the N_2 data which is opposite to that of O_2, i.e., the peak shifts to slightly smaller values of χ with increasing collision energy.

Unpublished results from this laboratory of the neutral cross sections for collisions of Cl^- with the rare gases Ne, Ar, Kr and Xe show the same general features of those found for these three molecular targets, and the maxima in those cross sections are located at χ -values that are essentially independent of collision energy.

The neutral results of CO, shown in Fig. 21, are strikingly different from those of the other molecular targets. At a collision energy of 64.6 eV, the cross section has a maximum at $\chi \approx 900$ eV-deg: the location of this maximum shifts to slightly larger values with increasing collision energy. In addition, there is a second maximum at the much smaller value of $\chi \approx 200$ eV-deg. Since this process (which is not present in the other systems) produces neutrals that are scattered at small angles, the contamination problem at small scattering angles is far more severe in the CO system. This is apparent in Fig. 21 where, after corrections for "no scattering gas" have been made, the peak at $\chi = 0$ is still comparable in magnitude to the one at $\chi \approx 200$ eV-deg. Measurements at energies above and below those shown in Fig. 21 show that the small χ -process is dominant at high collision energies but becomes small compared to the large χ -process at the lowest collision energies investigated. These observations tend to support the hypothesis that, in the case of CO, there are two distinct processes responsible for the production of neutral chlorine.

Examples of the relative differential cross sections for the elastic scattering of Cl^- by N_2, CO, and CO_2 are shown in Fig. 24. The differential cross sections all have the same general shape: Each

decreases smoothly, with increasing scattering angle, but shows a change in curvature (downward) at intermediate scattering angles. This feature is more apparent in the N_2 and CO cross sections than it is for CO_2, but is not nearly as pronounced in the molecular systems as it is for the rare gas targets studied previously.[19] These regions of downward curvature in the elastic cross sections are interpreted to be evidence for the onset of electron detachment which leads to the depletion of the elastic channel. The range of τ -values to which the majority of neutrals are scattered is, in each case, in reasonable agreement with the τ -values associated with the regions of downward curvature in the elastic cross sections.

For those trajectories which lead to detachment, the final scattering angles of the neutrals are determined by the amount of elastic scattering incurred before detachment takes place and the subsequent scattering on the outgoining neutral channel. If the ionic and neutral interactions are comparable in strength (which is a reasonable assumption) then they will contribute roughly equal amounts to the scattering. In this case the maxima in the neutral cross sections should be located at approximately the same τ -values as the apparent detachment thresholds in the elastic differential cross sections. This conclusion is consistent with the observations.

In summary, the absolute total detachment cross sections have been presented for Cl^- in collisions with various molecular species. It was found that the predominant energy threshold for electron detachment was well above the electron affinity of the negative ion, a result similar

to the experimental observations for the rare gas targets. The relative elastic and inelastic differential cross sections were in qualitative agreement with the predictions of a simple complex potential model.

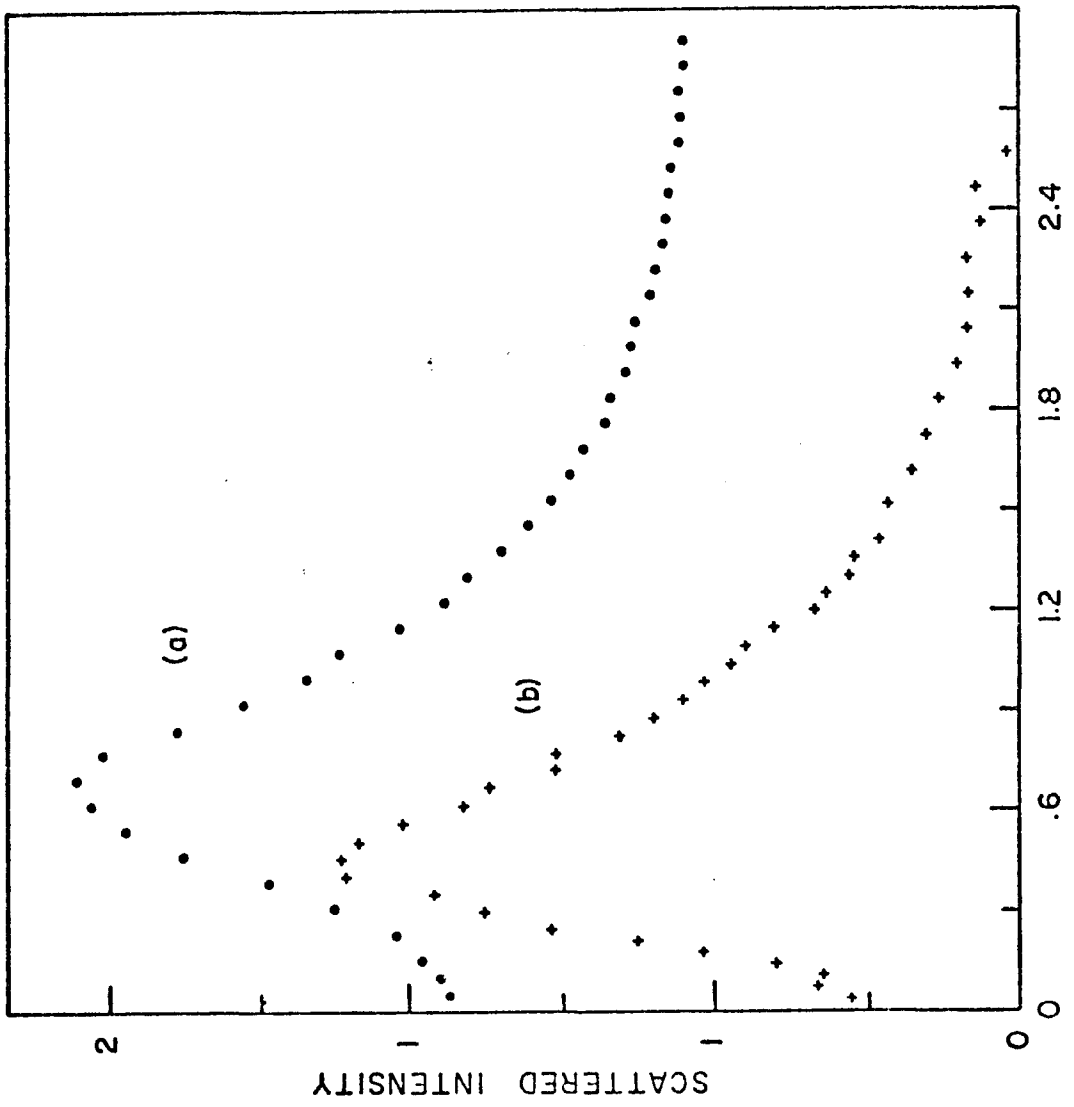

Figure 20. Relative differential cross sections for neutral chlorine as a function of $\tau = E\theta$ for the system $Cl + O_2$: (a) E_1 = 154 eV, (b) E_1 = 106 eV.

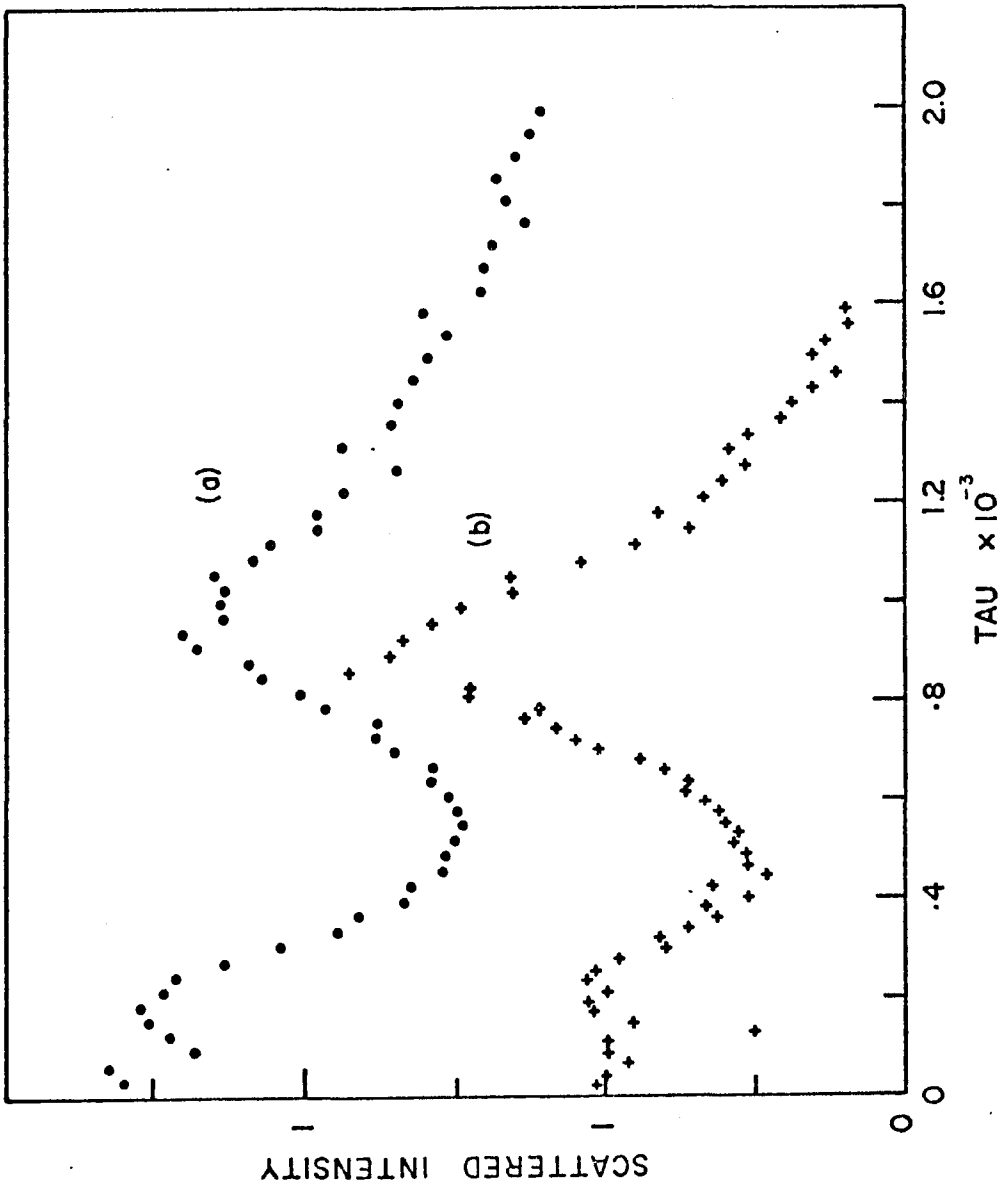

Figure 21. Relative differential cross sections for neutral chlorine as a function of $\gamma=E\theta$ for the system Cl^- + CO: (a) E_1 = 91 eV, (b) E_1 =66eV.

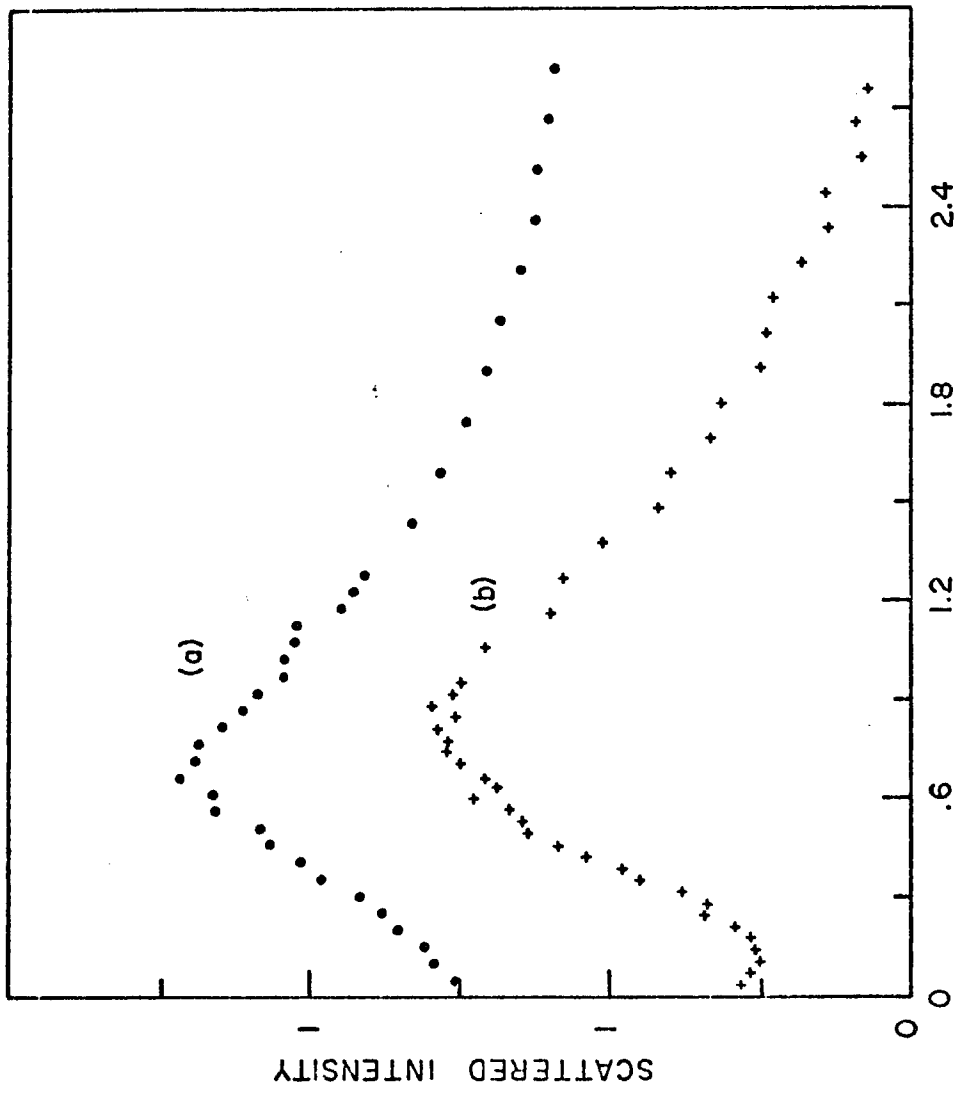

Figure 22. Relative differential cross sections for Cl for the system $Cl^- + N_2$: (a) E_1 = 154 eV, (b) E_1 = 106 eV.

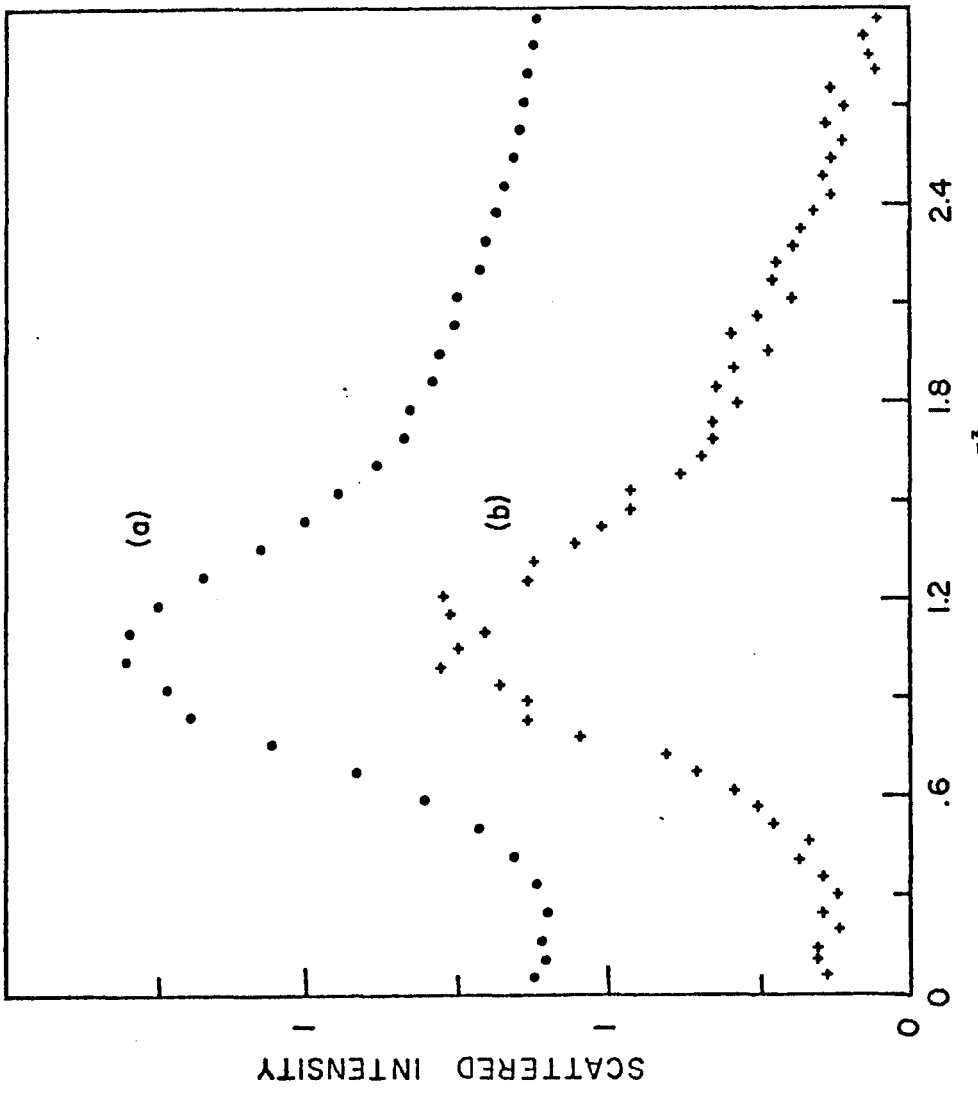

Figure 23. Relative differential cross sections for Cl for the system $Cl^- + CO_2$: (a) E_1 = 170 eV, (b) E_1 = 107 eV.

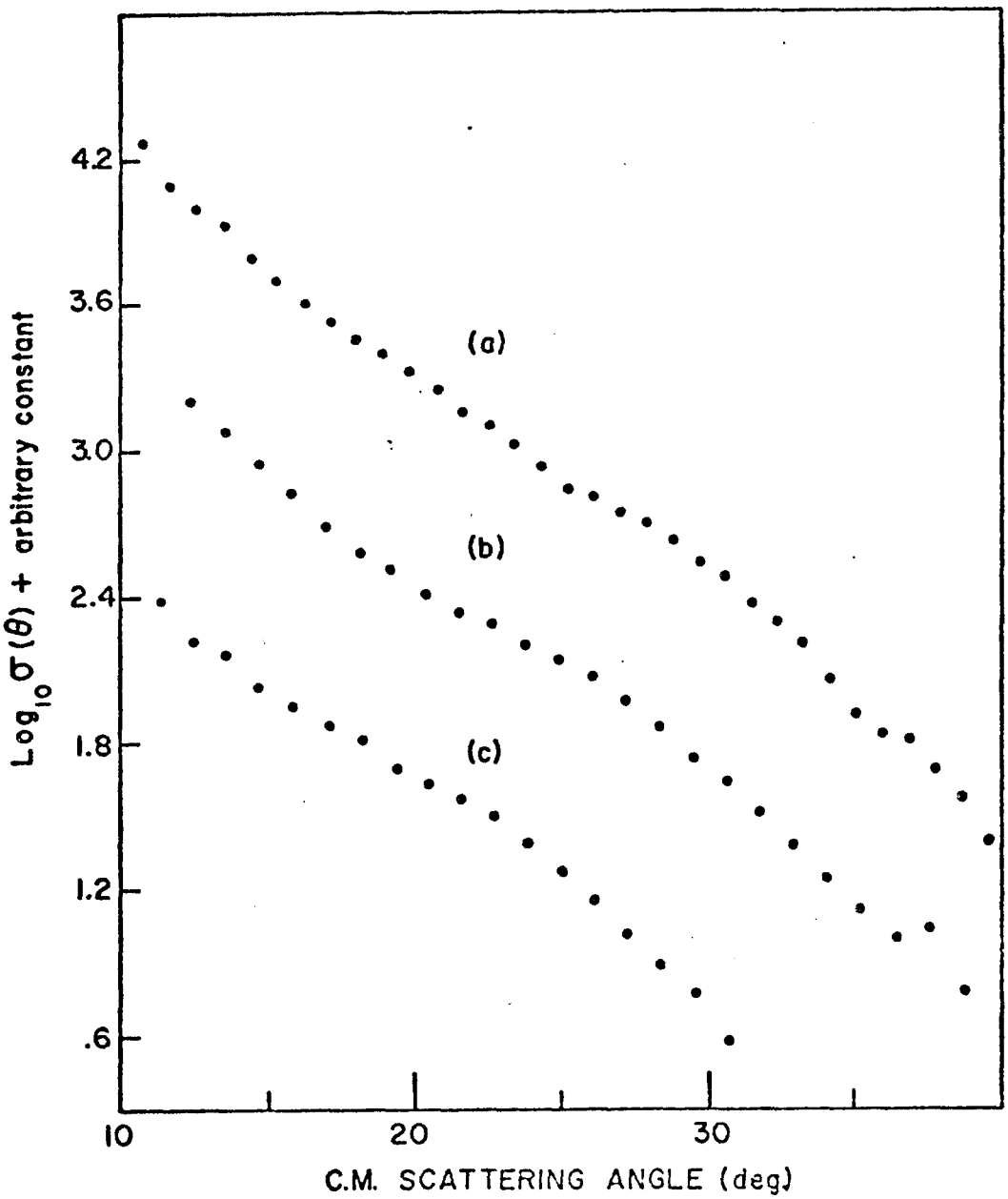

Figure 24. Relative differential cross sections for elastic scattering: (a) Cl^- + CO_2 at E = 42 eV, (b) Cl^- + CO at E = 46 eV, (c) Cl^- + N_2 at E = 47 eV. Here, E is the center of mass collision energy.

VI. RESULTS OF THE NEGATIVE ION-ALKALI ATOM EXPERIMENTS

Low energy relative differential cross section measurements were completed on the systems Cl^- + K, Na and H^- + Na. In addition to measuring the elastic cross sections, attempts were made to observe inelastic scattering.

In part A we will examine the alkali-halides and in part B the system H^- + Na. In both presentations a discussion of the possible coupling between various electronic states will be followed by the results of experimental observations.

A. Cl^- + Na and K

In chapter III it was shown that the systems NaCl and KCl have large dipole moments and are capable of supporting bound states for the negative molecular ions. With this in mind a schematic representation of the interaction potential can be constructed.

In Fig. 25 the interaction potentials for the anion, covalent and ionic states are shown. At large internuclear separations, the lowest covalent state is separated from the anion state by the E.A. of the halide. The covalent and the ionic state are separated by the difference between the ionization potential, I.P., of the alkali atom and the E.A. of the halide. The minimum splitting, at large internuclear separations, between the anion and ionic state is the ionization potential of the alkali atom. To note the energy separation corresponding to the lowest

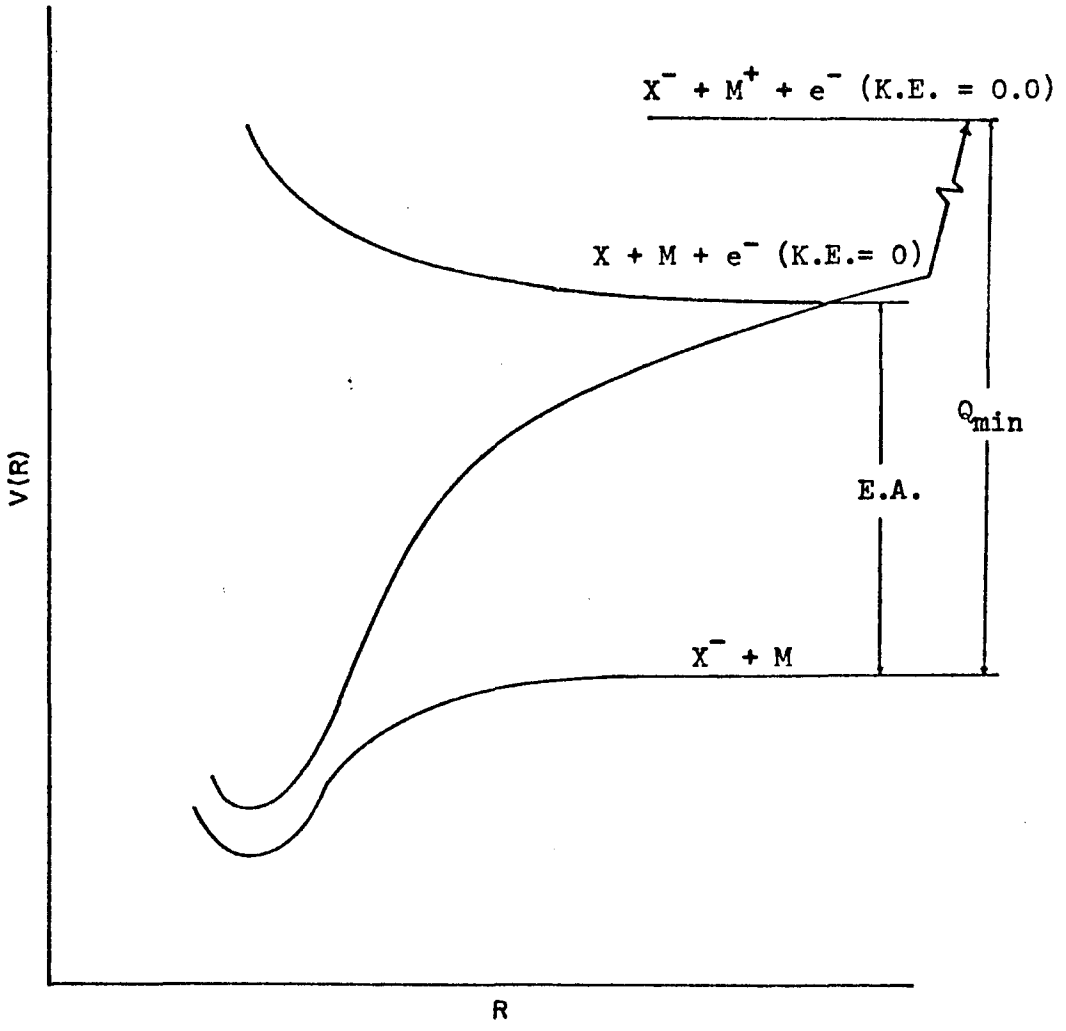

Figure 25. Schematic representation of the intermolecular potentials of the alkali - halide systems.

ionic state where the free electron has zero kinetic energy, minimum endothermicity for the reaction $X^- + M \rightarrow X^- + M^+ + e^-$ is defined as $Q_{min} = I.P.(M)$.

The potential curves have not been continued to small R values since their behavior is uncertain in this region. Following the incoming anion state we can enumerate a few possible outgoing channels:

a) elastic: $X^- + M \rightarrow X^- + M$

b) ionic inelastic: $X^- + M \rightarrow X^- + M^+ + e^-$

c) covalent inelastic: $X^- + M \rightarrow X + M + e^-$.

The molecular states for the outgoing channels (b) and (c) are known to cross. In the asymptotic limit the ionic state $M^+(^1S) + X^-(^1S)$ differs in energy from the covalent state $M(^2S_{1/2}) + X(^2P_{3/2})$ by the difference between the ionization potential and electron affinity. Since I.P. $>$ E.A. for all combinations of alkali and halide atoms, the difference is always positive and the ionic state will cross the repulsive covalent state. Both states have Σ^+ ground molecular states, thus in the Born-Oppenheimer representation there is at least one avoided crossing.

The coupling between the incoming anion state and outgoing ionic and covalent state is unknown for the $NaCl^-$ and KCl^- systems. We can, however, examine the ionic-covalent pseudocrossing. To predict the branching ratio for inelastic channels, we must consider the transition probabilities between states during the collision.

The collisional dissociation of alkali-halide molecules has been studied experimentally by Ewing, Milstein and Berry.[62] In a series of shock tube experiments they determined the branching ratios to the ionic

and covalent states. KCl underwent entirely ionic dissociation while NaCl was found to to be an immediate case, where both ionic and neutral products were observed.

The coupling between the ionic and covalent states at this avoided crossing has been investigated theoretically in recent literature.[63-66] In these discussions the Landau-Zener[67] model was sometimes employed to describe the inelastic collisions at the avoided crossings. We will use this model to determine the transition probabilities.

The Landau-Zener[67] model assumes all transitions take place in the region of the crossing point of the diabatic potential curves. The transition probability[67] is given as:

$$P = \exp\left[-2\pi\gamma\right] \tag{13}$$

where

$$\gamma = \frac{V_{12}^2(R_x)}{\hbar V(R_x)\left|d(V_{11}-V_{22})/dR\right|_{R=R_x}}$$

The diabatic potentials are V_{11} and V_{22} and the interaction potential is V_{12} evaluated at R_x; $V(R_x)$ is the radial velocity at the crossing point. The values of for collisional ionization of the alkali halides have been determined by Faist and Levine,[64] for a velocity equal to the threshold for ionization. If collisional detachment occurs then the probability that the system remains on the ionic diabatic curve is found from the parameters of Ref. 3 to be:

$$P\ (NaCl) \sim .992$$
$$P\ (KCl) \sim \text{unity}$$

In the same manner we can determine the probability of making a transition to the covalent curve at the crossing:

$$(1\text{-}P) \sim .008 \qquad (NaCl)$$

$$(1\text{-}P) \sim 3.5 \times 10^{-10} \qquad (KCl)$$

Finally, any inelastic transition which takes place during the collision has the highest probability of exiting on the ionic channel. The inelastically scattered Cl^- is expected to have a minimum endothermicity of 5.1 eV for the Na target and 4.3 eV for the K target. We have performed experiments to search for three possible outgoing channels:

a) elastic

$$Cl^- + M \rightarrow Cl^- + M,$$

b) ionic inelastic

$$Cl^- + M \rightarrow Cl^- + M^+ + e^-, \text{ and}$$

c) neutral inelastic

$$Cl^- + M \rightarrow Cl + M + e^-.$$

Before examining the data, it should be noted that it was necessary to correct the energy scale of these experiments due to the presence of large contact potentials. The collision chamber was stainless steel and heated at the bottom; because stainless steel has a low thermal conductivity there existed a decreasing temperature from the bottom to the top of the chamber. Thus, a layer of alkali atoms condensed onto the surface of the chamber.

When two dissimilar metals come in contact, the Fermi levels will reach equilibrium giving rise to a contact potential. If the work functions are different [in this case, ϕ (Na) < ϕ (S.S)] then the energy

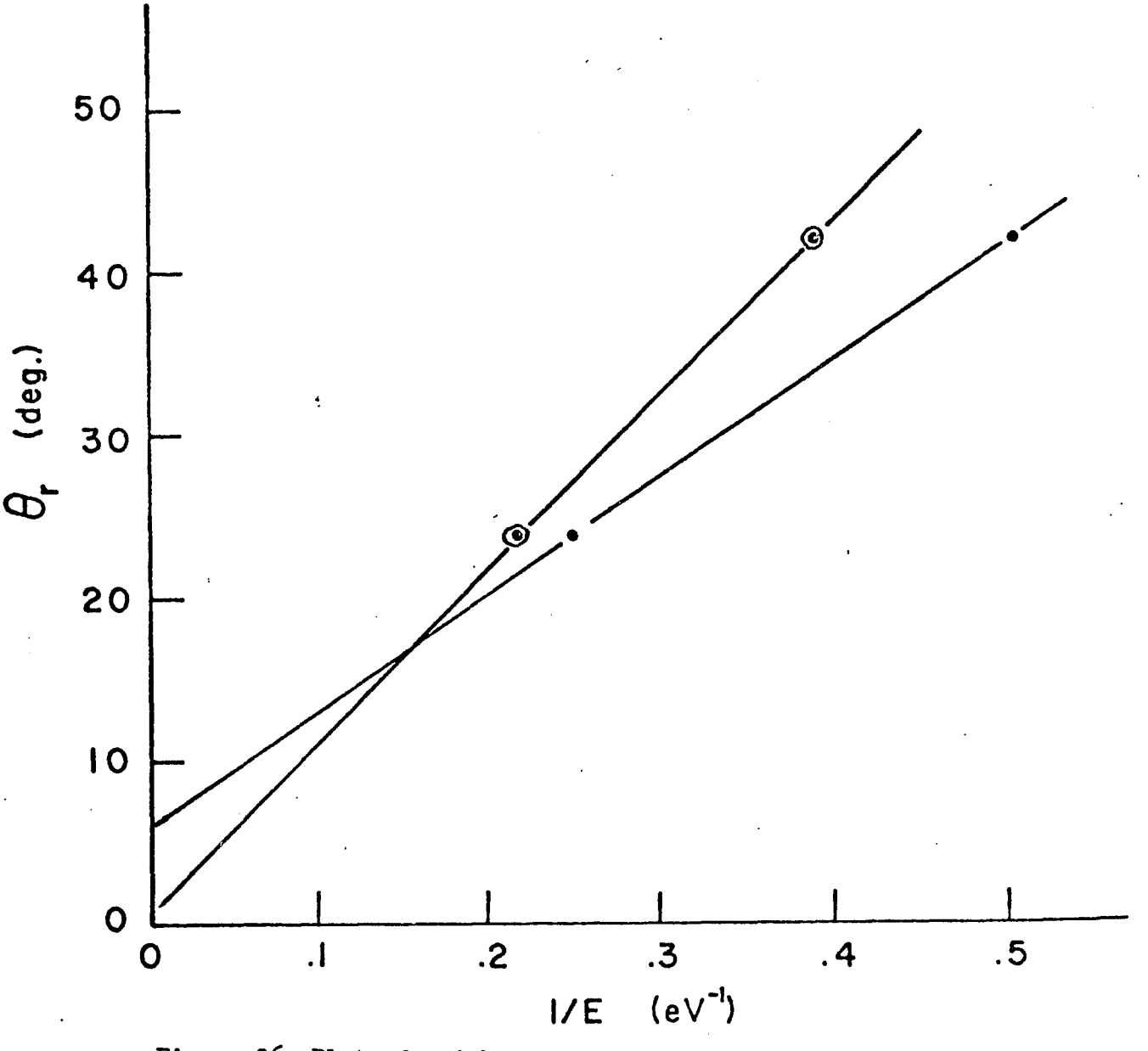

Figure 26. Plot of rainbow angle versus the inverse of relative collision energy for the Cl^- + Na system. The dots are the nominal energy and the circled dots have been adjusted upward by .6 eV.

levels of the electrons in the two metals are different. Consequently, the electrons can tunnel from one metal to the other with the Na becoming more positive and the stainless steel more negative. Finally, an equilibrium will be established in which the two Fermi levels coincide as a consequence of the potential rise (for electrons) across the gap associated with the surface charges. The potential rise is given by[68]:

$$eV = \phi(S.S) - \phi(Na)$$

where V is the contact potential. For the alkali targets used here the contact potential is positive and leads to an acceleration of the negative ion into the collision region; on leaving the collision chamber the ion is similarly decelerated. The change in ion energy is therefore not directly observable.

To determine the exact energy shift would require detailed knowledge of surface characteristics (contaminants, geometry, etc.) inside the collision chamber. This information is not available. However, we can determine indirectly the energy shift. For these bound state systems, the elastic differential cross sections exhibit typical rainbow phenomena. It is well known that the product E times θ_r is invariant with E. Thus we have plotted the rainbow angle, θ_r, versus the inverse of the relative energy, E. This is illustrated in Fig. 26 for the Cl^- + Na system. A straight line drawn through the two points should pass through the origin, since in this choice of parameters, the rainbow angle approaches zero for large energies. This was not the case and it was found that the laboratory energy must be adjusted upward by

1.5 eV to correct the energy scale for the contact potential. A similar result was found for the system Cl^- + K. This is in approximate agreement with estimates of the work functions for these metals.

The relative elastic differential cross sections were measured over a relative energy range of 4-60 eV. The results are shown in Figs. 27-28 for Cl^- + Na and K respectively. The data is presented in the form of a reduced cross section,

$$\rho = \theta_{c.m.} \times \tau_{el} \times \sin\theta_{c.m.} ,$$

and a reduced scattering angle $\tau = E_{c.m.} \times \theta_{c.m.}$. Smith, et al. have shown this representation is equivalent ot an expansion in impact parameter for the reduced angle.[69] Thus any prominent feature appearing at some value of τ which is invariant with energy depends on a unique impact parameter. The low energy experiments of Cl^- + Na and Cl^- + K both exhibit rainbow maxima at approximately 92 eV deg. The higher energy experiments show smoothly decreasing values of ρ for $\tau > \tau_r$ rainbow. If there was significant coupling to the direct electron detachment channel, the elastic scattered signal would be expected to show a distinct depletion. No such drop in the data is found; thus any coupling to the detachment channel is apparently small when compared to the elastic scattering.

A calculation was performed for the elastic differential cross sections of these systems and is shown as the solid line in Figs. 27-28. This calculation is the result of a partial wave analysis which uses the usual form of the scattering amplitude:[70,71]

$$f(\Theta) = \frac{1}{2ik} \sum_{l=o}^{\infty} (2l+1)\,(e^{2i\eta_l} - 1)\, P_l(\cos\Theta).$$

At a given scattering angle, the amplitude is a sum over angular momentum quantum numbers, where $P_l(\cos\Theta)$ are the Legendre Polynomials of order l, k is the wave number, and η_l is the phase shift experienced l^{th} partial wave.

The phase shifts are obtained in the JWKB approximation and have the form:

$$\eta_l = \frac{\pi}{2}(l + \tfrac{1}{2}) - kr_c + k \int_{rc}^{\infty} \left[\left(1 - \frac{V(R)}{E} - \frac{(l+\frac{1}{2})^2}{2\mu E r^2}\right)^{\frac{1}{2}} - 1\right] dr$$

where r_c is the classical turning point or outermost zero of the function

$$E - V(R) - \frac{(l+\frac{1}{2})^2}{2\ r_c^{\,2}}$$

The elastic differential cross section is defined as:

$$\frac{d\sigma(\Theta)}{d\Omega} = |f(\Theta)|^2.$$

The integral in the equation defining the phase shift is evaluated by standard numerical techniques, and at least 4000 partial waves are required for the partial wave sum to converge. The scattering amplitude was calculated in one-half degree steps and the resulting differential cross section was convoluted by a gaussian with a width of six degrees. This convolution removed the high frequency oscillations in the cross sections and was an approximation to the effects of doppler broadening.[55]

It is convenient to use an analytic form for the potential to carry out the phase shift calculations. Jordan and Wendoloski[39] have calculated a potential for $NaCl^-$ around the region of potential miminim,

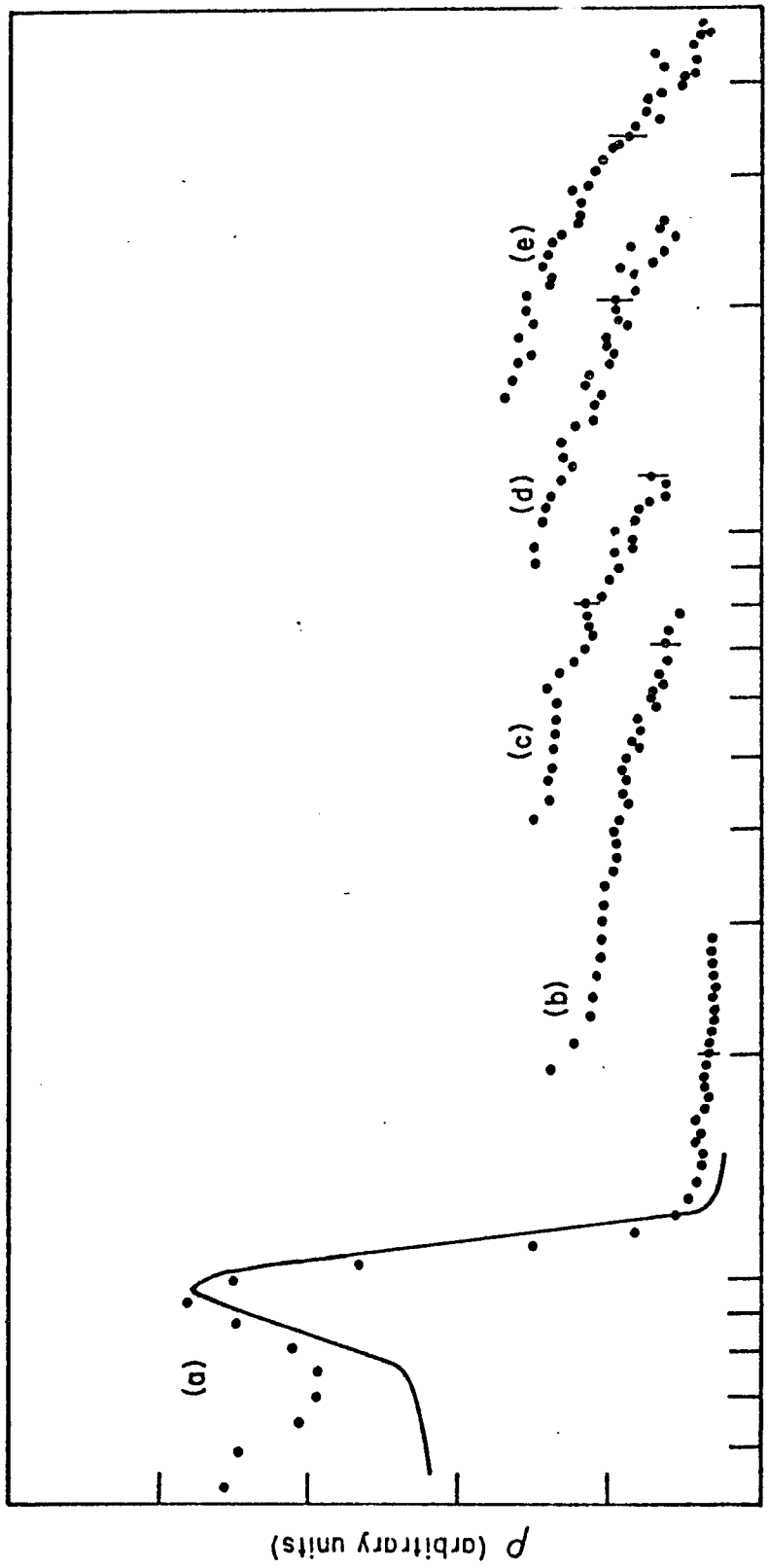

Figure 27. Relative reduced elastic scattering cross sections as a function of reduced scattering angle for the system $Cl^- + Na$ are shown for relative collision energies of (a) 4.6 eV, (b) 13 eV, (c) 21 eV, (d) 40 eV, (e) 60 eV. The solid line is the result of a calculation.

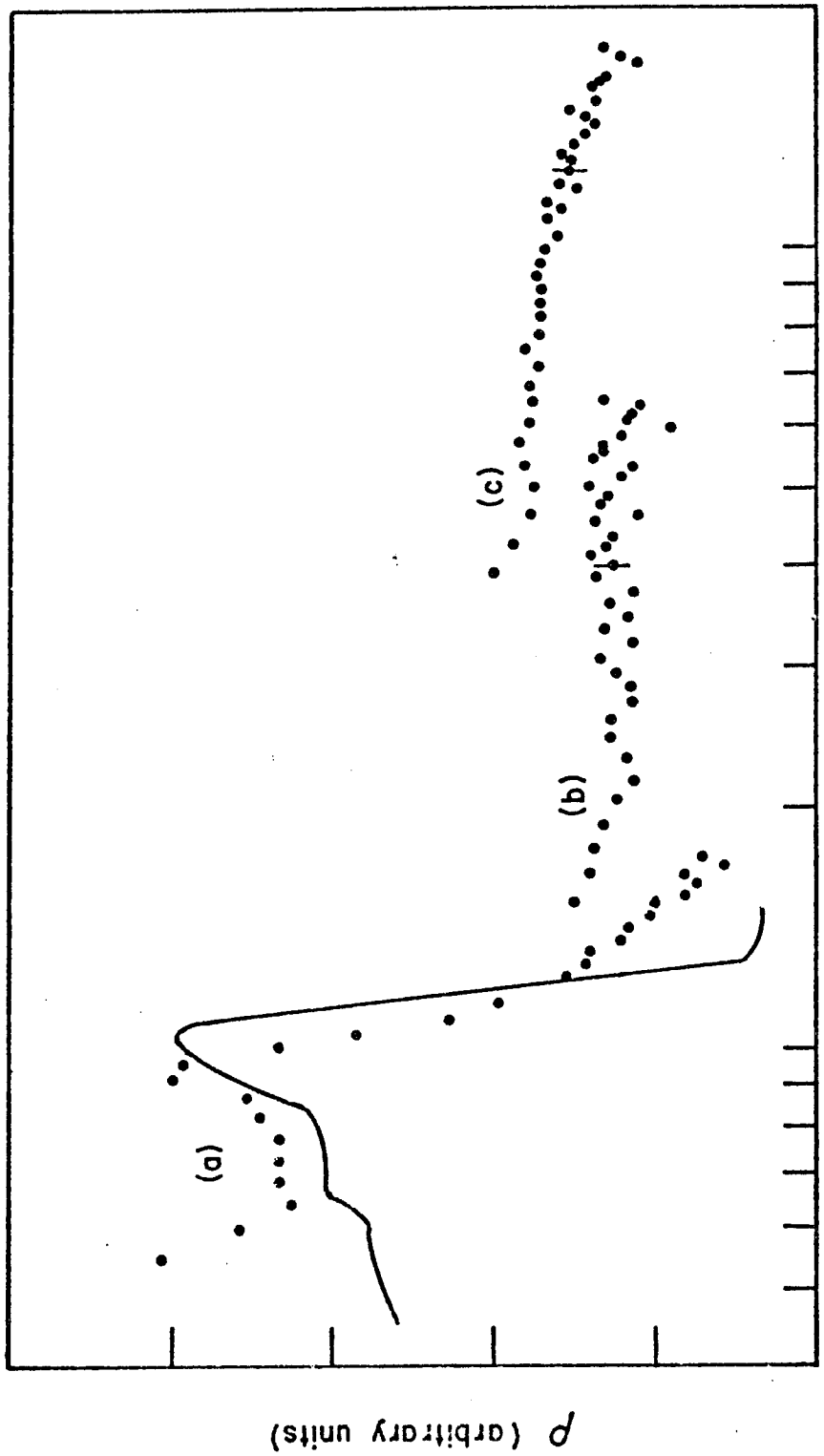

Figure 28. Relative reduced elastic scattering cross sections as a function of reduced scattering angle for the system Cl^- + K are shown for relative collision energies of (a) 4.8 eV, (b) 14 eV, (c) 38 eV. The solid line is the result of a calculation.

and we have fitted their calculations with a potential of the form:

$$V(R) = \sum_{i=1}^{3} A_i \, e^{-\alpha_i R} \qquad (14)$$

This potential has been made to agree with the calculation in the region of the potential minimum, and agree with the large polariziability term for large R. The parameters are listed in Table 3. The calculation included in Fig. 27 and as can be seen agreement between the calculation and experiment is excellent.

No intermolecular potential calculations exist for the KCl^- system. However, this system (and others) has been studied by de Vreugd, et al.[72] over an energy range of 500-5000 eV and an angular range of 0-5 milli-randians. We have used a potential with the same form as Eq. 14 which was determined by de Vreugd, et al.[72] by an inversion of their scattering data. Their potential parameters are listed in Table 3. As can be seen in Fig. 28, the agreement is only fair as the calculated rainbow maximum is approximately 13% higher in γ than the observed maximum.

A search was made for fast neutrals which would be the result of an inelastic transition having an exit channel along the covalent state. Experiments were done for laboratory energies up to 150 eV and scattering angles from zero to forty degrees; no fast neutrals were detected. In the higher energy experiments of de Vreugd, et al.[72] there was no evidence that fast neutrals were produced.

We have shown that if the negative ion undergoes collisional detachment then the final outgoing state has the highest probability of exiting on the ionic channel. Attempts were made to observe these

inelastically scattered negative ions. Typical results for the two systmes are shown in Fig. 28 where the relative intensity of scattered ions is plotted as a function of final kinetic energy of these ions. The peaks labeled Q = 0, correspond to the elastically scattered ions. The position of the minimum energy loss, Q_{min}, which is equal to an inelastic transition to the lowest ionic state, is also shown. For Cl^- + Na no inelastic signal was detectable at the energy and angle illustrated or at any other combination of energy or angle over a laboratory range of 10-150 eV and 0-40 degrees. The Cl^- + K data does show a signal which is $\sim$10% of the elastic scattering peak at a position equal to an inelastic transition to the lowest ionic state.

In summary, for our energy range, the cross section for ion pair formation or collisional detachment appears to be small.

B. H^- + Na

The bound state of the negative molecular ion and the lowest ionic and covalent states for this alkali-hydride system can also be described qualitatively by Fig. 24. The same discussion used in describing the possible couplings between states of the alkali-halide system is applicable for collisions of H^- + Na, but we will see that only transitions to the covalent state are expected.

In Chapter III we reported on the calculation of Karo, Gardner and Hiskes[42] (KGH) for the anion state, ($X^2\Sigma^+$) NaH^-, and the neutral, ($X^1\Sigma^+$) NaH state. A reasonable extrapolation of their potentials to internuclear separations less than $3a_o$ show the two states crossing at

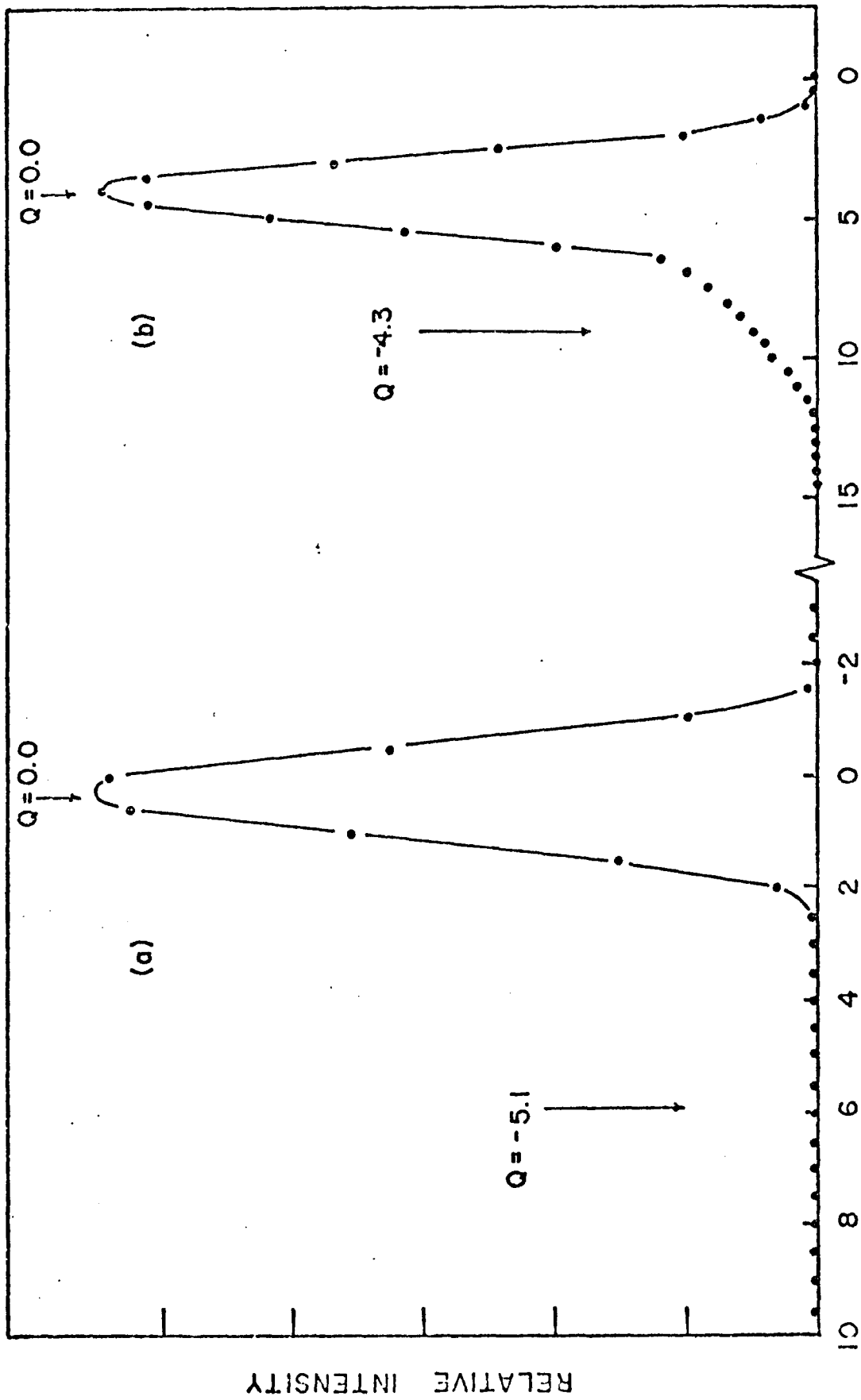

Figure 29. Relative intensity of scattered ions as a function of final kinetic energy of the ions: (a) Cl^- + Na at E_1 = 51 eV and Θ_{Lab} = 5 degrees; (b) Cl^- + K at E_1 = 71 eV and Θ_{Lab} = 15 degrees.

$R \simeq 2.6a_o$. This crossing may provide for a fairly large transition probability between the anion and neutral state. The interaction between the anion and ionic state is unknown, but it is possible to compute the coupling between the ionic and covalent states for any inelastic outgoing channels.

The Landau-Zener model can be used to determine the transition probability between the ionic and covalent states. The forms of the diabatic curves at the crossing are unavailable for this system but we can estimate the difference in the slopes at the crossing. At the large internuclear crossing of these curves,[63] $R_x = 7.55a_o$, the covalent curve is approximately flat and the ionic curve has a coulombic dependence thus the force term in the Landau-Zener formula (Eq. 13) is

$$\left| \frac{d(V_{11} - V_{22})}{dR} \right|_{R = R_x} \approx \frac{1}{R_x^2} \quad .$$

The interaction between the diabatic states can be approximated by one-half the splitting between the adiabatic states and this splitting has been determined by Numrich and Truhlar[66] and Grice and Herschbach[63] (GH) to be 0.564 eV and 1.54 eV respectively. Using the GH splitting[63] the diabatic transition probability at a relative collision energy of 10 eV is

$$P \sim \exp\left[\frac{-\pi (\Delta V_{ad})^2 R_x^2}{2h\, V(R_x)} \right] = 5 \times 10^{-7} \quad .$$

With such a small diabatic transition probability, the outgoing channel is expected to follow almost exclusively the covalent state if collisional detachment occurs.

Relative elastic differential cross section measurements were made for H^- colliding with Na for relative collision energies around 10 eV. The results of two experiments at 8.8 eV and 11.3 eV are shown in Fig. 31. Prominent rainbow maxima are observable at τ = 80 eV-deg. The solid line shown below the experimental results is the result of a partial wave calculation which uses JWKB phase shifts as discussed in the previous sections.

To evaluate the JWKB phase shifts we have employed the intermolecular calculation of KGH.[42] Starting with a Morse potential[73] for the NaH $[V^o(R)]$ potential curve, the anion curve $[V^-(R)]$ is constructed using the equation:

$$V^-(R) = V^o(R) - \Delta(R) + 0.09 \text{ eV}, \qquad (14)$$

where $\Delta(R)$ is the difference between the neutral and anion potential curves as calculated by KGH.[42] The constant 0.09 eV is needed to yield the correct electron affinity for hydrogen at infinite separation. The calculated points of the above potential is fitted to a function of the form:

$$V(R) = \sum_{i=1}^{3} A_i \, e^{-\alpha_i R}, \text{ and} \qquad (15)$$

the resulting potential parameters are contained in Table 3. The neutral Morse potential, the calculated anion potential and the fitted form of the anion potential are all shown in Fig. 30. Both the dissociation energy and equilibrium separation values computed by Eq. 2 agree well with those calculated by Jordan, et al.[39] As can be seen, the partial wave calculation is in excellent agreement with the experimental results.

A classical deflection function calculation is included in Fig. 31, based on the potential of Eq. 15 and a relative collision energy of 10 eV. The rainbow feature is located at a reduced scattering angle of $\gamma_r \sim 95$ eV-deg. The reduced angle which corresponds to a classical turning point of $2.6a_o$ is found to be 150 eV-deg, which is well outside the rainbow region. As stated earlier the KGH[42] calculations show the anion and neutral states merging at $R_x \sim 2.6a_o$, thus for collisions which sample a smaller internuclear separation than this crossing, the collisional detachment channel may become significant.

The experimental results at 15 eV are illustrated in Fig. 31(d) and exhibit a break in the reduced cross section at a reduced scattering angle of $\gamma \simeq 150$ eV-deg. This sudden depletion of the elastic scattering signal is typical of systems undergoing collisional induced electron detachment. No such break was observable in the lower energy experiments and is presumably due to the rather low signal-to-noise ratios for $\gamma \geq$ 120 eV-deg. in these experiments.

Unfortunately, the neutral particle detector was not installed during the H^- + Na experiments, therefore the inelastic neutral differential cross sections could not be measured. A search for inelastic ionic transitions undergoing a minimum energy loss of at least 5.1 eV over a laboratory energy range up to 70 eV and an angular range out to 40 degrees in the laboratory revealed no detectable signal above the normal background levels. In this energy range the reaction $H^- + Na \rightarrow H^- + Na^+ + e^-$ is believed to have a very small cross section.

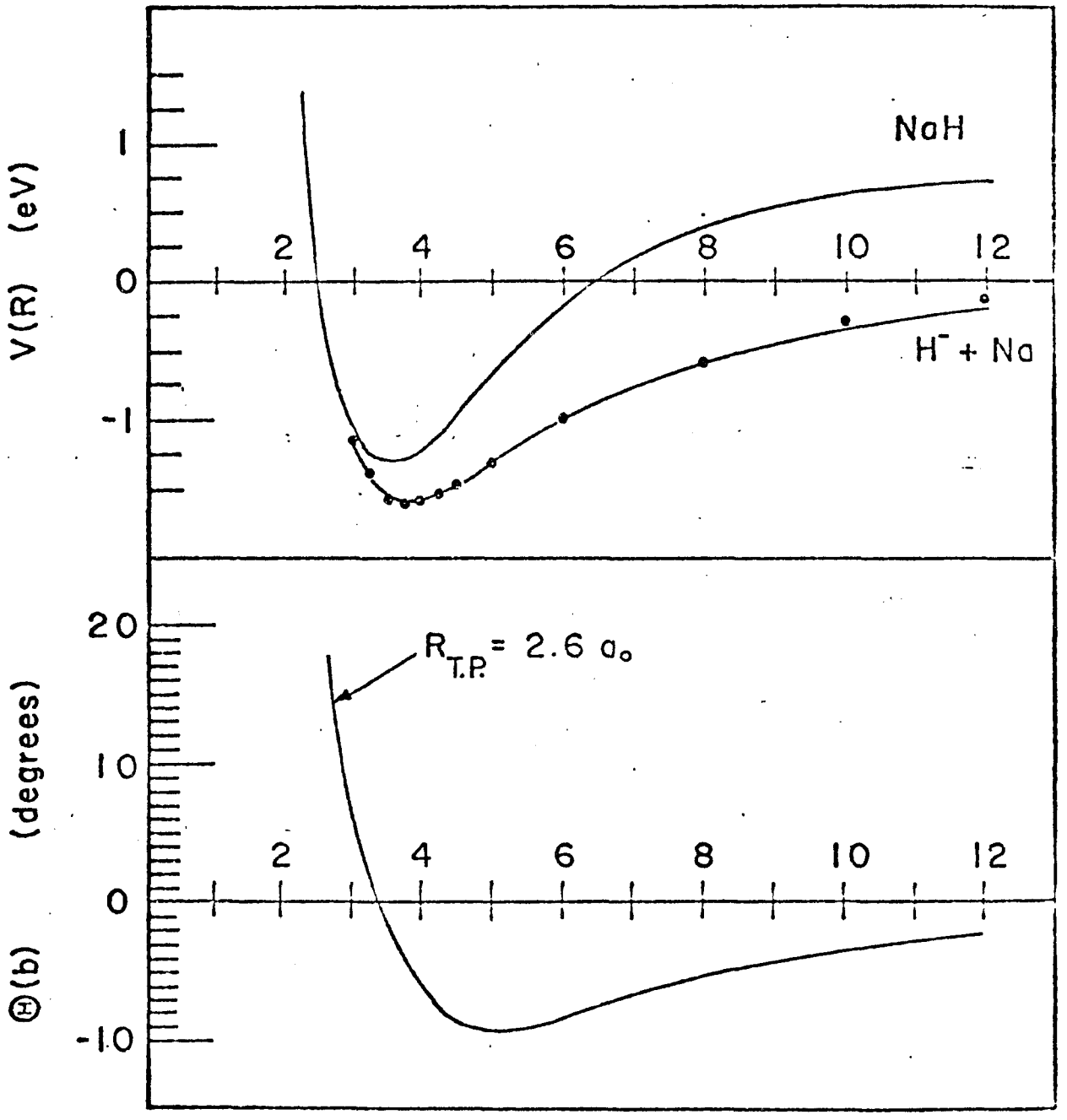

Figure 30. Intermolecular potentials for NaH and NaH^-. The points are from Eq. 14 and the solid line fitted to those points is given by Eq. 15. The classical deflection is calculated for a relative collision energy of 10 eV. The abcissae are in atomic units.

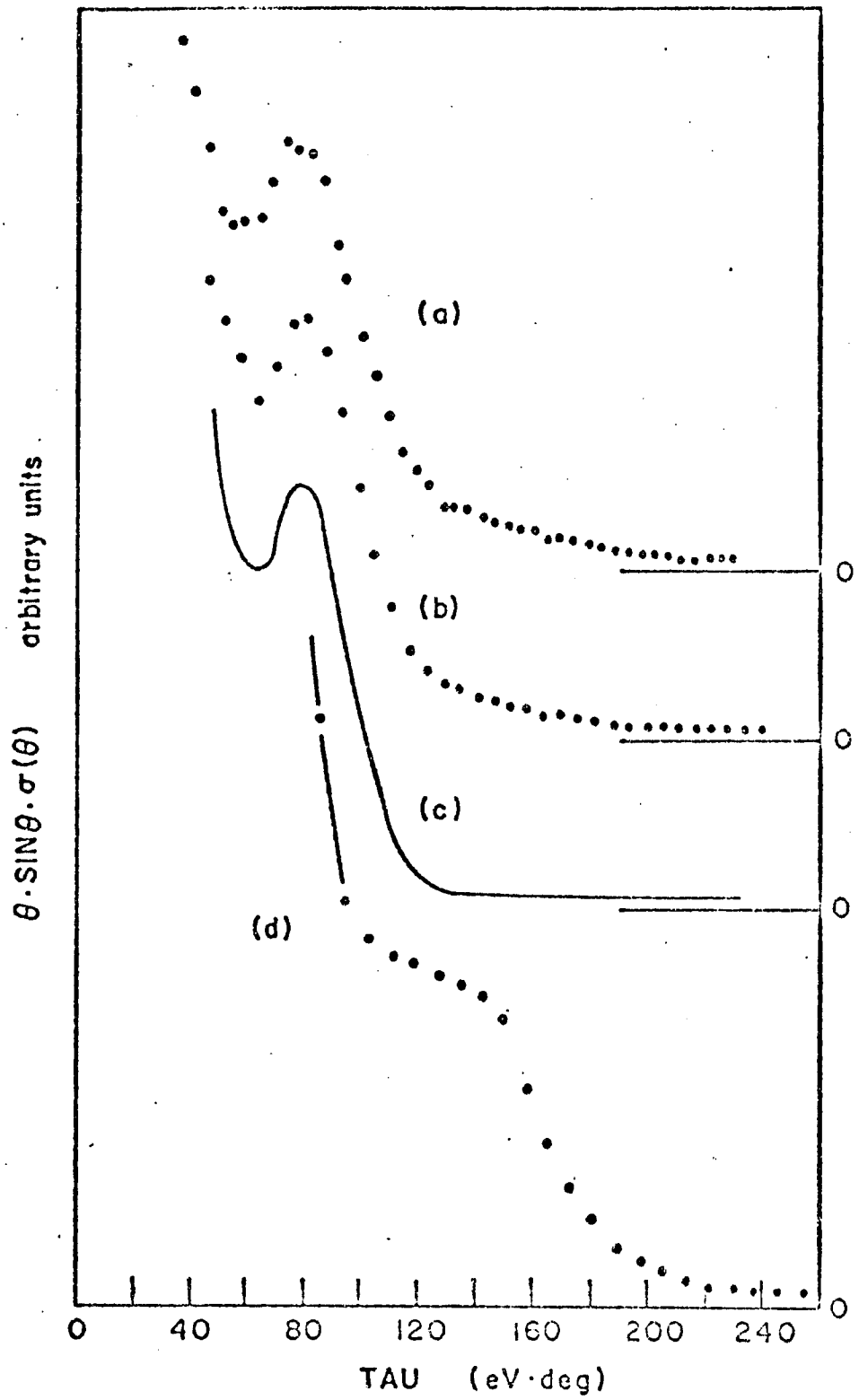

Figure 31. Differential cross section for elastic scattering -- (a) and (b) are the experimental results for E = 8.8 and 11.3 eV, respectively; (c) is a calculation based upon the potential of Eq. 15; (d) is an experiment for E = 15.1 eV. The relative scale of the ordinate for (d) is about six times that for the other figures.

As mentioned earlier, the location of the calculated rainbow maximum is invariant with respect to the reduced angle, γ. We can, therefore estimate an upper limit for the uncertainty (due to contact potentials) in the collision energy:

$$\begin{aligned} \text{If } \gamma_1 &= E_{1exp}\theta_1 = (E_{1true} + \delta E)\theta_1 \\ \text{and } \gamma_2 &= E_{2exp}\theta_2 = (E_{2true} + \delta E)\theta_2 \end{aligned} \tag{16}$$

are defined as the experimentally observed rainbow maxima for two different experiments, then the uncertainty in energy can be estimated as:

$$\delta E = \frac{\delta\gamma}{\theta_2 - \theta_1} \tag{17}$$

where $\delta\gamma$ is the limiting accuracy for which the experimental rainbow maxima can be said to be invariant with collision energy. From Fig. 31(a) and (b) δE can be estimated to be approximately 1.5 eV.

Although the agreement is excellent between the experimental results and calculation this is only a fair test of the potential calculations since the energy scale is uncertain by approximately 15% and the agreement may only be fortuitous.

VII. SUMMARY AND CONCLUSION

Measurements of the absolute total detachment cross sections for collisions of negative ions of chlorine with the rare gases and various molecular targets have been presented. Particular emphasis has been placed on the energetic threshold for collisional detachment. For all of the reactants the predominant threshold for detachment was found to occur for relative collision energies well above the electron affinity of the chlorine atom. A local complex potential model has been used to describe the collisional detachment channel, and a calculation based on this model was in good agreement with the experimental results for the targets Ne, Ar and Kr. The qualitative features of the experimental results for the molecular targets were in general agreement with the ideas of the complex potential model except for the observed inverse isotope effect for the targets D_2 and H_2. The experimental results presented are of sufficient detail and accuracy to provide a good test for ab initio potential calculations of negative molecular ions as well as models which may be employed to describe collisional detachment.

Relative differential cross section measurements were presented for collisions of negative ions of chlorine with various molecular targets. Both the elastic differential cross section and the differential cross section for the production of neutral chlorine atoms were in qualitative agreement with the ideas of a local complex potential. The neutral spectra of the CO target exhibited evidence for two

distinct scattering channels leading to detachment; this was the only system exhibiting this phenomena.

Further differential cross section measurements were made for the systems Cl^- + Na, K and H^- + Na. The large dipole moments of these alkali-halide and alkali-hydride molecules means that their anions form bound molecular states: this is evidenced by the rainbow features observed in the elastic differential cross sections of Cl^- + Na(K) and H^- + Na.

The rainbow features observed in the elastic differential cross sections of Cl^- (H^-) + Na are consistent with calculated cross sections based upon recent calculations of the intermolecular potentials.

A search for inelastic transitions which result from collisions of Cl^- + Na, K led to scant evidence for such transitions: in particular, there was no evidence for detachment for $0 < \gamma < 5000$ eV-deg. The system H^- + Na exhibited evidence of collisional detachment in the realtive elastic differential cross section. It is thought that for $\gamma > 150$ eV-deg, the collisional detachment may be significant.

TABLE I

	Dipole Moments[a]
NaCl	9.00D
KCl	10.27D
NaH	6.96D

(a) Dipole moments taken from NBS, Technical Note 438, December 1967, M. Krauss, Editor.

TABLE II

Potential Parameters for Cl^- + X from Ref. 19

for a Potential of the form $W(R) = V(R) - i/2\Gamma(R)$

$$V(R) = \frac{Ae^{-BR}}{R}$$

$$\Gamma(R) = \begin{cases} 0 & R > R_x \\ F(R_x - R)^{3/2} & R_1 \leq R \leq R_x \\ F(R_x - R_1)^{3/2} & R < R_1 \end{cases}$$

Target	$A(eVa_o)$	$B(1/a_o)$	$R_x(O_o)$	$F(eV/a_o^{1.5})$	$R_1(a_o)$	Width[a]
Kr	3062	1.39	3.46	4.6	3.00	
Ar	2530	1.37	3.39	5.4	3.07	1.08
Ne	826	1.39	2.61	4.8	2.40	1.30
He						1.42

(a) Refers to width used in deconvolution of the data.

TABLE III

	α_1 ($1/a_o$)	α_2 ($1/a_o$)	α_3 ($1/a_o$)	A_1 (eV)	A_2 (eV)	A_3 (eV)	R_m (a_o)	$D_e(x^-m)$ (eV)
$NaCl^-$	1.50	.70	.40	839.278	-33.046	-4.899	4.77	1.25
KCl^-	1.35	.63	.36	992.36	-35.125	-5.6266	5.29	1.30
NaH^-	1.45	.576	.15	152.5	-11.8	-1.43	3.8	1.62

REFERENCES

1. Chemistry of the Ionosphere, A. D. Danilov, Plenum Press (New York, London, 1970) pp. 129-171.
2. Negative Ions, H. S. W. Massey, Cambridge University Press (Cambridge, 1976) pp. 663-682.
3. F. E. Spenser, Jr., J. C. Hendric, Jr. and D. Bienstock, Paper VII 4, 13th Symposium on Engineering Aspects of Magnetohydrodynamics (26-28 March 1973).
4. Proc. of the Symposium on Production and Neutralization of Negative Hydrogen Ions and Beams (26-30 September 1977) Brookhaven National Lab.
5. W. G. Graham, LBL-Report 6837, September 1977.
6. W. Aberth, J. R. Peterson, RSI, 38, 745 (1967).
7. G. P. Lawrence, R. K. Beauchamp, J. L. McRibbin, Nucl. Instr. and Meth. 32, 357 (1965).
8. A. Persky, E. F. Greene, A. Kupperman, JCP, 49, 2347 (1968);
   G. I. Dimor, G. V. Raslyakov, Sov. Phys.-Tech. Phys. 17, 90 (1972);
   N. Koshira, E. Vietzke, G. Z'ellerman, RSI, 48, 171 (1977);
   J. Cheung, Private communication;
   P. Dittner and S. Datz, JCP, 68, 2451 (1978).
9. K. R. Spangenberg, Vacuum Tubes, McGraw-Hill (1948);
   F. H. Read, A. Adams, J. R. Soto Mortiel, J. Phys. E, 4, 625 (1972);
   A. Adams, F. H. Read, J. Phys. E, 5, 156 (1972).

10. F. Rosebury, Handbook of Electron Tube and Vacuum Techniques, Addison-Wesley Publ. Inc., Reading, Mass., p. 147, 1965.

11. A. L. Hughes, V. Rajansky, Phys. Rev. 34, 284 (1929);
A. L. Hughes, J. H. McMillen, Phys. Rev. 34, 291 (1929).

12. K. R. Wilson, Lawrence Radiation Lab, Report UCRL-11605, (1964);
W. Paul, H. P. Reinhardt, U. von Zahn, Z. Phys. 152, 143 (1958).

13. C. S. Leffel, RSI, 35, 1615 (1964).

14. J. Adams, B. W. Monley, IEEE Trans. Nucl. Sc. NS-13, 88 (1966);
K. C. Schmidt, Bendix Technical Applications Note 9803, April 25, 1969.

15. R. Morgenstern, D. C. Lorents, J. R. Peterson, R. E. Olson, Phys. Rev. A8, 2372 (1973).

16. W. Wien, Vech. dtsch. phys. Geo. 16, 165 (1892).

17. Thanks to F. A. Kern of NASA-Langley.

18. W. Frebin, C. Schlier, K. Strein and E. Telroy, JCP 67, 5505 (1977);
B. von Zyl, G. E. Chamberlain and G. H. Dunn, J. Vac. Sci. Tech. 13, 721 (1976).

19. R. L. Champion and L. D. Doverspike, Phys. Rev. A13, 609 (1976).

20. F. Reif, Fundamentals of Statistical and Thermal Physics, p. 277, McGraw-Hill (New York, 1965).

21. B. T. Smith, W. R. Edwards III, L. D. Doverspike and R. L. Champion, Phys. Rev. A, to be published September 1978.

22. D. W. Sida, Proc. Phys. Soc. A68, 240 (1955).

23. M. R. C. McDowell and G. Peach, Proc. Phys. Soc. 74, 463 (1959).

24. Yu. N. Demkov, JETP, 19, 762 (1964).

25. G. B. Lapantseva and O. B. Firsov, JETP, 23, 648 (1966).

26. A. Z. Devdariani, Teo. Math. Fiz. 11, 213 (1972); JETP, 18, 255 (1973).

27. V. Esaulov, D. Dhuicq and C. P. Gauyacq, J. Phys. B., 11, 1049 (1978).

28. S. K. Lam, J. B. Delos, R. L. Champion and L. D. Doverspike, Phys. Rev. A9, 1828 (1974).

29. R. L. Champion, L. D. Doverspike and S. K. Lam, Phys. Rev. A13, 617 (1976).

30. S. K. Lam, Ph.D. Thesis (College of William and Mary, 1975).

31. J. Mizuno and J. C. Y. Chen, Phys. Rev. 187, 167 (1969); Phys. Rev. A4, 1500 (1971);

J. C. Y. Chen, Advances in Radiation Chemistry, edited by M. Curton and J. L. Magee (Wiley, New York 1968), Vol. 1, p. 245ff.

32. T. F. O'Malley, Phys. Rev. 155, 59 (1967).

33. R. E. Olson and B. Liu, Phys. Rev. A17, 1568 (1978).

34. E. Clementi and C. Roetti, At. Data Nucl. Data Tables, 14, 177 (1974).

35. R. P. Saxon and B. Liu, J. Chem. Phys. 64, 3291 (1976).

36. K. D. Jordan and W. Luken, JCP, 64, 2760 (1976).

37. K. D. Jordan, JCP, 65, 1214 (1976).

38. M. R. H. Rudge, J. Phys. B11, 1497 (1978).

39. K. D. Jordan and J. J. Wendoloski, Mol. Phys. 35, 223 (1978).

40. K. D. Jordan, K. M. Griffing, J. Kenney, E. L. Anderson and J. Simons, JCP, 64, 4730 (1976).

41. J. Simons, Ann. Rev. Phys. Chem. 28, 15 (1977) and references cited in this review article.

42. A. M. Karo, M. Gardner and J. R. Hiskes, JCP, 68, 1942 (1978).

43. R. F. Wallis, R. Herman and H. W. Milnes, Jour. Mol. Spec. 4, 51 (1960).

44. A. S. Wightman, Ph.D. Thesis (Princeton University, 1949).

45. M. H. Mittleman and V. P. Myerscough, Phys. Lett. 23, 545 (1966).

46. J. E. Turner and K. Fox, Phys. Lett. 23, 547 (1966).

47. O. H. Crawford, Proc. Phys. Soc. 91, 279 (1967).

48. O. H. Crawford, Mol. Phys. 20, 585 (1971); Mol. Phys. 26, 139 (1973); JCP, 68, 4968 (1977).

49. J. L. Carlsten, J. R. Peterson and W. C. Lineberger, Chem. Phys. Lett. 37, 5 (1976).

50. V. O. Rosenbaum, Z. Naturforschg. 13a, 838 (1958); Z. Naturforschg. 13a, 842 (1958).

51. Y. F. Bydin and V. M. Dukel'skii, JETP, 4, 474 (1957).

52. A. J. H. Boerboom, H. Von Dop and J. Los, Physica 46, 458 (1970).

53. Y. F. Bydin, ZhETF Pis'ma, 6, 857 (1967).

54. J. Fayeton, D. Dhuicq and M. Barat, J. Phys. B11, 1267 (1978).

55. P. J. Chantry, JCP, 55, 2746 (1971).

56. G. E. Ioup and B. S. Thomas, JCP, 46, 3959 (1967) and G. E. Ioup, Ph.D. Dissertation (University of Florida, 1968), unpublished. The computer program for the deconvolution was adapted from that given in the latter reference.

57. In the period between the measurements of Ref. II-14 and the present measurements, the capacitance manometer was returned to the manufacturer for major repair and recalibration.

58. R. L. Champion, L. D. Doverspike and S. K. Lam, Phys. Rev. A13, 617 (1976).

59. J. Cheung and S. Datz, private communication.

60. D. Vogt and K. H. Opiela, Phys. Lett. 54A, 331 (1975).

61. G. I. Dimov and G. V. Roslyakov, Sov. Phys. Tech. Phys. 17, 90 (1972).

62. J. J. Ewing, R. Milstein and R. S. Berry, JCP, 54, 1752 (1971).

63. R. Grice and D. R. Herschbach, Mol. Phys. 27, 159 (1974).

64. M. B. Faist and R. D. Levine, JCP, 64, 2953 (1976).

65. M. B. Faist, B. R. Johnson and R. D. Levine, Chem. Phys. Lett. 32, 1 (1975).

66. R. W. Numrich and D. G. Truhlar, J. Phys. Chem. 79, 2745 (1975).

67. Molecular Collision Theory, M. S. Child, Academic Press, London and New York, 1974, pp. 161-166.

68. A. J. Dekker, Solid State Physics, (Prentice-Hall, 1960), pp. 230-231.

69. F. T. Smith, R. P. Marchi and K. G. Dedrich, Phys. Rev. 150 (1977).

70. H. Foxen and J. Holtsmark, Z. Phys. 45, 307 (1927).

71. Lord Rayleigh, Theory of Sound, Vol. 2, 1896, Macmillan, New York and London.

72. C. de Vreugd, R. W. Wignaendts van Resandt, J. Los, B. T. Smith and R. L. Champion, to be published in Chem. Phys.

73. AIP Handbook, Third Edition, pp. 7-170.